# Neuronal extracellular vesicles and associated microRNAs induce circuit connectivity downstream BDNF
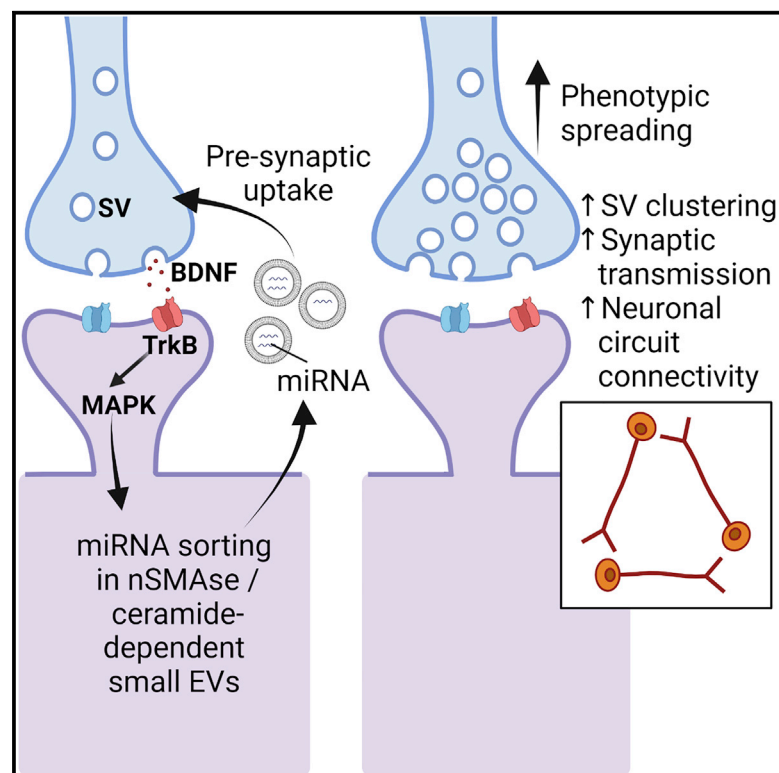
## Graphical abstract



## Highlights

- BDNF induces the sorting of specific miRNAs in small extracellular vesicles (EVs)

- BDNF-induced EVs increase excitatory synapse clustering via miRNA-218, -132, -690

- EVs transmit synaptic phenotypes to secondary neurons downstream BDNF

- BDNF-induced EVs promote synchronous neuronal network activity

## Authors

Anna Antoniou, Loic Auderset, Lalit Kaurani, ..., Jan Gründemann, Andre Fischer, Anja Schneider

## Correspondence

anna.antoniou@dzne.de (A.A.),
anja.schneider@dzne.de (A.S.)

## In brief

Antoniou et al. describe a mechanism of brain-derived neurotrophic factor (BDNF)-mediated synapse formation via the transfer of neuronal EVs and miRNA cargo. BDNF-stimulated EVs increased synaptic vesicle clustering at pre-synaptic terminals and enhanced synaptic activity and neuronal circuit connectivity, likely by inducing their own propagation within neuronal circuits.

CellPress

## Article

# Neuronal extracellular vesicles and associated microRNAs induce circuit connectivity downstream BDNF

Anna Antoniou,[1,2,*] Loic Auderset,[1,2] Lalit Kaurani,[3,4] Eva Sebastian,[2] Yuzhou Zeng,[1,2] Maria Allahham,[5,6] Silvia Cases-Cunillera,[7] Susanne Schoch,[7] Jan Gründemann,[2] Andre Fischer,[3,4] and Anja Schneider[1,2,8,*]

[1]Department for Neurodegenerative Diseases and Geriatric Psychiatry, University of Bonn Medical Center, 53127 Bonn, Germany
[2]German Center for Neurodegenerative Diseases (DZNE), 53127 Bonn, Germany
[3]Department of Psychiatry and Psychotherapy, University Medical Center Göttingen, 37075 Göttingen, Germany
[4]Department for Systems Medicine and Epigenetics in Neurodegenerative Diseases, German Center for Neurodegenerative Diseases (DZNE) Göttingen, 37075 Göttingen, Germany
[5]Institute of Bio- and Geosciences 1, Forschungszentrum Jülich, 52428 Jülich, Germany
[6]Aachen Biology and Biotechnology, RWTH Aachen University, 52056 Aachen, Germany
[7]Section for Translational Epilepsy Research, Department of Neuropathology, University of Bonn Medical Center, 53127 Bonn, Germany
[8]Lead contact
*Correspondence: anna.antoniou@dzne.de (A.A.), anja.schneider@dzne.de (A.S.)
https://doi.org/10.1016/j.celrep.2023.112063

## SUMMARY

Extracellular vesicles (EVs) have emerged as mediators of cellular communication, in part via the delivery of associated microRNAs (miRNAs), small non-coding RNAs that regulate gene expression. We show that brain-derived neurotrophic factor (BDNF) mediates the sorting of miR-132-5p, miR-218-5p, and miR-690 in neuron-derived EVs. BDNF-induced EVs in turn increase excitatory synapse formation in recipient hippocampal neurons, which is dependent on the inter-neuronal delivery of these miRNAs. Transcriptomic analysis further indicates the differential expression of developmental and synaptogenesis-related genes by BDNF-induced EVs, many of which are predicted targets of miR-132-5p, miR-218-5p, and miR-690. Furthermore, BDNF-induced EVs up-regulate synaptic vesicle (SV) clustering in a transmissible manner, thereby increasing synaptic transmission and synchronous neuronal activity. As BDNF and EV-miRNAs miR-218 and miR-132 were previously implicated in neuropsychiatric disorders such as anxiety and depression, our results contribute to a better understanding of disorders characterized by aberrant neural circuit connectivity.

## INTRODUCTION

Extracellular vesicles (EVs) are lipid membrane-enclosed vesicles that have recently emerged as important regulators of development, adaptation, and homeostasis in several biological systems.[1] In the brain, EVs were shown to mediate communication between neurons and non-neuronal cells[2–4] and have been implicated in the spreading of misfolded, aggregating proteins in neurodegenerative disease models.[5–9] Inter-neuronal transfer of EVs was also shown to be important for the pruning of excitatory synapses[4,10] and modulation of inhibitory neurotransmission.[11] Nevertheless, how inter-neuronal EVs transfer may be implicated in structural and functional plasticity, and whether they modulate neural circuit connectivity is still largely unexplored.

EVs are enriched in small non-coding RNAs like microRNAs (miRNAs), in particular small EVs originating from intracellular endosomes.[12] miRNAs inhibit the translation of messenger RNA (mRNA) targets based on imperfect base pairing in the cytoplasm. The local regulation of translation by miRNAs is thought to be important for rapid modifications of the neuronal proteome, which is critical during dendrite maturation, growth cone naviga-

tion, and synaptic plasticity.[13–16] Indeed, miRNA production and activity is tightly regulated by plasticity-inducing stimulation and neuromodulators such as brain-derived neurotrophic factor (BDNF),[15,17–19] a major neurotrophin that has been implicated in many neuropsychiatric disorders such as depression and anxiety.[20] BDNF signaling via its high-affinity receptor, *tropomyosin kinase receptor B* (TrkB) both mediates and modulates long-term plasticity, for instance via regulation of transcriptional and translational gene expression. BDNF itself is not mobile in the extracellular space and therefore only participates in localized signaling,[21] which is thought to be critical for the fine-tuning of neuronal circuits.[20] Even though the molecular mechanisms of BDNF-dependent synapse formation and plasticity have been extensively studied, how BDNF signaling guides the formation and maintenance of neural circuits is still unclear.

We hereby describe a mechanism of BDNF-dependent neural circuit formation via EVs and associated miRNAs. BDNF specifically up-regulated the abundance of miRNAs previously implicated in synaptogenesis and neuropsychiatric disorders, miR-218 and miR-132,[22] in small EVs derived from primary neurons. Transcriptomics analysis of neurons treated with BDNF-induced
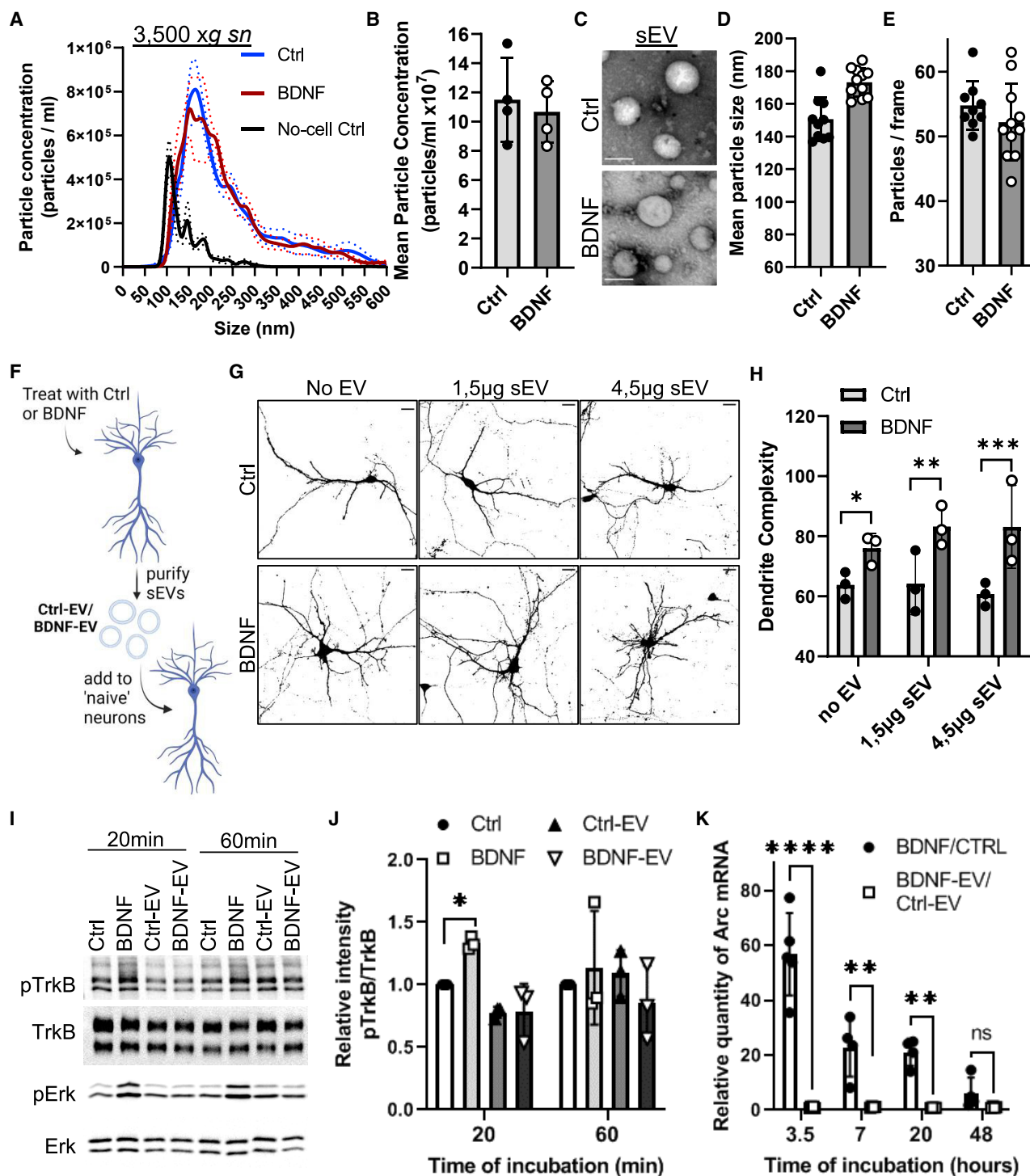
**Figure 1. BDNF-EVs increase dendrite complexity**

(A) Cleared cell culture supernatants (3,500 × $g$ sn) from control (Ctrl) vehicle-treated or BDNF-treated cortical neurons (7 DIV) were processed in NTA. Non-conditioned, fresh culture medium ("no-cell ctrl") was used as a control. Data are represented as mean ± SEM; n = 4.

(B) Mean particle concentration of extracellular supernatants as in (A); n = 4.

(C) Scanning transmission electron microscopy (STEM) images of sEVs obtained from Ctrl- or BDNF-treated neurons; scale bars are 100 nm.

(D) Mean particle size of sEVs in STEM micrographs; n = 10–11.

(E) The average number of sEVs in STEM micrographs; n = 10–11.

EVs revealed the differential expression of genes related to excitatory synapse formation, many of which were targets of these miRNAs. Consistently, the activity and EV-mediated delivery of miR-218-5p, miR-132-5p, and miR-690 was necessary and sufficient for BDNF-dependent excitatory synapse formation in hippocampal neurons. EVs derived from BDNF-treated, but not control-treated, donor neurons induced the clustering of synaptic vesicle (SV) markers opposing dendrites, a phenotype that was transmissible to secondary hippocampal neurons. Furthermore, BDNF-induced EVs increased the amplitude of synaptic calcium transients and increased synchronous neuronal activity, suggesting that EV transmission regulates neuronal network connectivity. Overall, this work provides insight into the establishment of neural circuits by BDNF that could better explain its role in neural circuit formation and the pathophysiology of several neuropsychiatric disorders.

## RESULTS

### BDNF does not influence the abundance of neuron-secreted EVs

EVs represent a broad class of secretory vesicles that includes exosomes, 50–150 nm vesicles originating from multi-vesicular endosomes (MVEs), and microvesicles, which are derived from the plasma membrane and range from 100 nm up to 1 μm in size. Because EV preparations are never homogeneous,[1,12] we refer to EVs based on their size distribution rather than biogenesis. Using ultra-centrifugation (Figure S1A), we isolated small and medium-sized EVs (sEVs and mEVs, respectively) from mouse primary cortical neurons at 5–6 days in vitro (DIV). SEVs and mEVs had a peak particle size of 168.5 ± 5.6 and 196.6 ± 8.7 nm and mean particle concentration of 3.66e8 ± 9e7 and 2.17e8 ± 6.22e7 particles/mL, respectively, measured using nanoparticle tracking analysis (NTA) (Figure S1B). Depletion of mitotic cells using cytosine arabinoside (AraC) did not affect sEV yield (Figure S1C), as our primary cultures only contained 2%–3% of GFAP-positive glia cells (Figure S1D), suggesting that sEVs were mainly derived from post-mitotic neurons. Moreover, inhibition of ceramide production by the neutral sphingomyelinase (N-SMase) inhibitor GW4869 decreased particle concentration in sEVs and non-fractionated cell supernatants, but not in mEVs (Figures S1E and S1F), and indicated that nearly half of sEVs are derived from ceramide-dependent biogenesis pathways.[23–25]

To investigate whether BDNF plays a role in sEV secretion, we performed an acute, short-term treatment of cortical neurons with BDNF and collected sEVs 16 h later. BDNF did not affect the yield or size distribution of bulk secreted fractions (3,500 × g Sn) (Figure S1A) measured using NTA (Figures 1A and 1B), which was consistent with scanning transmission electron microscopy (STEM) analysis of sEV fractions (Figures 1C–1E and S1G). In addition, BDNF did not change the total protein or RNA concentration of purified sEVs (Figures S1H and S1I) or the relative abundance of the sEV proteins TSG101 and Flotilin-2 (Figure S1J). Furthermore, neither tetrodotoxin (TTX) nor bicuculline (Bic) affected the concentration of sEVs in NTA (Figure S1K), suggesting that neuronal activity does not influence EV secretion at this developmental stage (5–6 DIV), contrary to what was previously shown in older (15 DIV) neurons.[26]

### BDNF-stimulated, but not control-stimulated, sEVs increase dendrite complexity in recipient neurons without activating BDNF-TrkB signaling pathways

BDNF is a well-known regulator of neuronal dendrite morphogenesis, particularly in the hippocampus.[20,21] We therefore examined whether sEVs are implicated in BDNF-dependent morphological changes at dendrites. SEVs derived from control (Ctrl)- or BDNF-treated cortical neurons (hereafter referred to as Ctrl-EVs and BDNF-EVs, respectively) were incubated with hippocampal neurons at 6–7 DIV, and dendrite complexity was quantified using Sholl analysis 3 days later (Figure 1F). BDNF-EVs increased neuronal dendrite outgrowth in a non-dose-dependent manner, whereas Ctrl-EVs had no effect at either dosage (Figures 1G, 1H, S2A, and S2B). We then investigated whether this observed increase in dendrite complexity is due to the co-fractionation of endogenous or exogenous BDNF with sEVs by treating neurons with BDNF, myc, or myc-BDNF and analyzing protein composition in sEVs and donor cell lysates (CLs) by western blotting. BDNF-EV fractions did not contain BDNF, as neither BDNF, myc-BDNF, nor myc were detectable in sEV fractions (Figure S2C). Consistently, incubation of hippocampal neurons with BDNF-EVs for 20 or 60 min did not lead to the phosphorylation of TrkB or the downstream kinases ERK and AKT (Figures 1I, 1J, and S2D–S2F), and neither ERK phosphorylation nor mature BDNF could be detected in BDNF-EV-recipient neurons for up to 3 h of incubation (Figures S2G and S2H). Moreover, unlike BDNF, BDNF-EVs did not induce TrkB-dependent transcriptional induction of the plasticity-related Arc mRNA[27] for up to 48 h following treatment (Figure 1K). Therefore, BDNF-EVs promote dendrite outgrowth in hippocampal neurons via a mechanism that is distinct from BDNF-TrkB signaling.

---

(F) Diagram depicting workflow for functional sEV assays.

(G) Thresholded images of dsRed-expressing hippocampal neurons treated with either Ctrl or BDNF (100 ng/mL, 20min) ("no EV"), and Ctrl-EVs or BDNF-EVs as shown in (F), and fixed 3 days later; scale bars are 20 μm.

(H) Dendrite complexity of neurons treated as in (G) was calculated using Sholl analysis in three independent experiments; n = 3, two-way ANOVA, *p = 0.04; **p = 0.006; ***p = 0.002.

(I) Western blot of cell lysates derived from Ctrl-, BDNF-, Ctrl-EV-, or BDNF-EV-treated hippocampal neurons. Cells were lysed 20 or 60 min after treatment and immunoblotted with antibodies against total or phosphorylated (p) TrkB and (p)ERK.

(J) Quantification of (I). The relative intensity of pTrkB was normalized to total TrkB and Ctrl vehicle in each independent experiment; n = 3, *p = 0.04 in two-way ANOVA.

(K) BDNF or BDNF-EV fold changes in Arc in hippocampal neurons. Mature Arc mRNA levels were quantified by qPCR, and values were normalized to total RNA concentration and GAPDH; n = 5, two-way ANOVA, **p < 0.01, ***p < 0.0001.
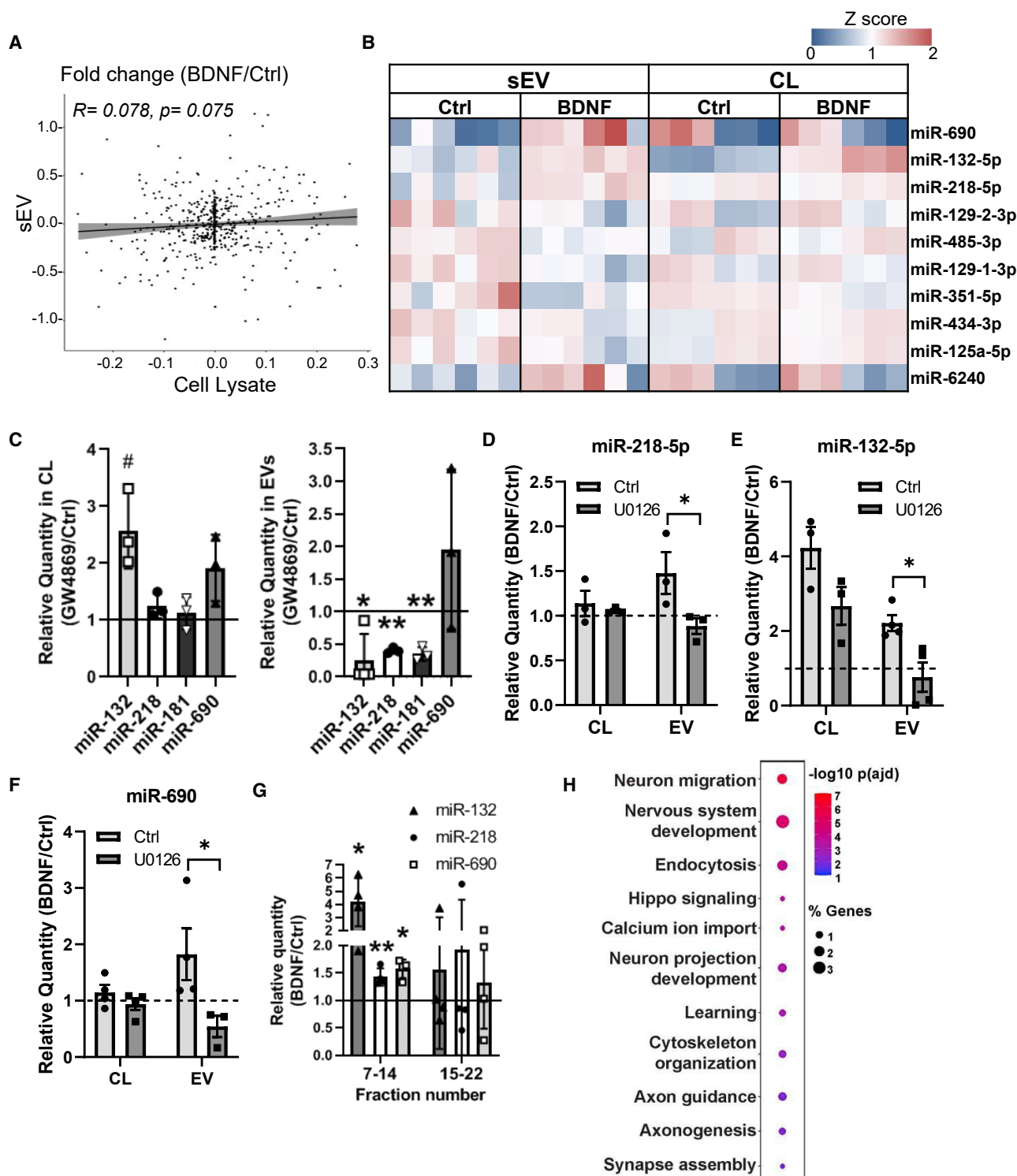
See also Figures S1 and S2.

**Figure 2. BDNF regulates the sorting of sEV-miRNAs**

(A) BDNF-induced fold changes in miRNA abundance in sEVs and cell lysates. Depicted are Pearson's correlation *R* and p value.

(B) Heatmap depicting the levels of the top 10 regulated sEV-miRNAs in decreasing order of significance and corresponding changes in cell lysates (CLs). Values were normalized to the base mean for each miRNA; n = 6.

(C) Relative miRNA quantity in cell lysates (left) and sEVs (right) was quantified in qRT-PCR following treatment of donor neurons with GW4869 or control vehicle; n = 3–4, *p = 0.03, **p < 0.01, Student's t test (heteroscedastic).

*(legend continued on next page)*

## BDNF induces the sorting of specific miRNAs in sEVs

As BDNF regulates miRNA biogenesis,[15,17,28] we were prompted to investigate whether BDNF also regulates the sorting of miR-NAs into sEVs. To this end, we isolated CLs and corresponding sEVs from Ctrl- and BDNF-treated cortical neurons and performed next-generation small RNA sequencing (NGS). Principle-component analysis (PCA) revealed the differential clustering of Ctrl- and BDNF-treated samples in both CLs and sEVs (Figure S3A). To our surprise, there was no correlation in BDNF fold changes in miRNA abundance between CLs and sEVs (Figures 2A and 2B), indicating the specific sorting of miRNAs into sEVs. Among the sEV miRNAs exhibiting the most significant changes in abundance, miR-218-5p, miR-690, and miR-351-5p are regulated in sEVs only; miR-132-5p is up-regulated in both compartments; and miR-129-2-3p is down-regulated in sEVs and up-regulated in CLs (Figures 2B and S3B; see also Table S1). Since some miRNAs are reportedly found in cell culture media components such as serum, we examined the presence of miR-132-5p, miR-218-5p, miR-690, and miR-181a-5p in non-conditioned primary neuronal culture media. These miRNAs were largely absent from neuronal culture media (Figure S3D), likely due to the absence of serum. With the exception of miR-690, these miRNAs were also depleted from sEVs following inhibition of N-SMase activity by GW4869 (Figure 2C).

We selected the three significantly up-regulated miRNAs miR-132-5p, miR-218-5p, and miR-690 (adjusted p < 0.05; Table S1) for further analysis. Treatment of donor neurons with the specific ERK inhibitor U0126 completely blocked the BDNF-induced increase of these miRNAs in sEVs without affecting their abundance donor cells (Figures 2D–2F), indicating the specificity of this pathway. Importantly, neither BDNF nor U0126 treatment changed the concentration or size distribution of purified sEVs (Figures S3D and S3E). Extracellular RNAs have been reported in non-membrane-associated fractions, particularly in the circulation.[29] We therefore examined BDNF-induced fold changes in miRNA abundance in sEV-enriched and protein-enriched fractions using size-exclusion chromatography (fraction number 7–14 and 15–22, respectively). Although both fractions contained miRNAs, the BDNF-induced up-regulation of miR-132-5p, miR-218-5p, and miR-690 was only evident in sEVs (Figure 2G). To examine the potential functions of BDNF-regulated sEV-miRNAs, we performed target prediction analysis for miR-132-5p, miR-218-5p, and miR-690 for neuronal transcripts with binding sites at the 3′ untranslated region (3′ UTR). Gene set enrichment analysis of putative miRNA targets common to at least 2 of these miRNAs (up to 1,163 transcripts) showed an enrichment of genes related to nervous system development and included the terms "neuron migration," "neuron projection development," "axon guidance," and "synapse assembly" (Figure 2H). Furthermore, many of these transcripts are present at

dendrites, synapses, or axons, as indicated by cellular component enrichment analysis (Figure S3F).

## BDNF-induced EVs differentially regulate the abundance of transcripts related to synaptogenesis

To gain insight into the potential regulation of gene expression by BDNF-EVs, we investigated BDNF- and BDNF-EV-dependent changes in the transcriptome using whole-cell RNA sequencing. Although changes in gene expression induced by BDNF-EVs were overall smaller than those triggered by BDNF (Figures 3A and S4A), we observed bidirectional changes in the abundance of several transcripts that did not simply reflect BDNF treatment (Table S2). Gene Ontology analysis of BDNF-EV-induced genes revealed the enrichment of biological pathways related to nervous system development, cholesterol biosynthesis, cell migration, and axon guidance (Figure 3B), whereas BDNF treatment alone induced pathways mainly related to the organization of the cytoskeleton, glutamate receptor activity, and synaptic plasticity (Figure S4B). Closer inspection of genes induced by BDNF-EVs revealed several positive regulators of glutamatergic synaptogenesis such as Sema4a, -6c, and -7a,[30–32] Wnt7a and -b,[33] and the calcium-inducible transcription factor NeuroD2[34] (Table S3). Moreover, genes down-regulated in response to BDNF-EVs were related to nervous system development and transcriptional regulation (Figure 3B; Table S3). Approximately 30% of significantly down-regulated genes are predicted targets of BDNF-regulated sEV miRNAs miR-218-5p, miR-132-5p, and/or miR-690 (Figure 3C) and include developmental regulators of gene expression such as Crem[35] and negative regulators of synaptogenesis such as Sema5a[36] and Slit2[37] (Table S4). These data thus indicate a role for BDNF-EVs as developmental regulators of synapse formation via the transfer of associated miRNAs.

## The combined activity of sEV-miRNAs is important for BDNF-dependent dendrite outgrowth

To investigate whether miRNAs mediate BDNF-EV-dependent structural changes at dendrites, we examined whether the endogenous activity of significantly up-regulated SEV miRNAs is necessary for BDNF-dependent dendritogenesis using anti-sense locked nucleic acid (LNA)-based miRNA inhibitors. Hippocampal neurons were transfected with dsRed and miRNA inhibitors for either miR-Ctrl (30 nM) or for miR-218-5p, miR-132-5p, and miR-690 individually (15 nM each) or in combination (30 nM total). Neurons were then treated with BDNF and imaged 3 days later (Figure 4A). Dendrite complexity was assessed using Sholl analysis, and fold changes in BDNF-mediated dendritogenesis were compared between each condition. Although inhibition of individual miRNAs did not significantly affect BDNF-induced changes in dendrite complexity, co-inhibition of miR-132-5p and

(D–F) BDNF fold changes in miRNA quantity in cell lysates and sEVs in the presence of the MAPK inhibitor U0126 or control. Relative values were normalized to miR-181a-5p reference miRNA; n = 3–4, *p < 0.05, two-way ANOVA.
(G) Relative abundance of EV-miRNAs in Ctrl or BDNF-induced sEVs or non-vesicular fractions isolated by size-exclusion chromatography (fractions 7–14 and 15–22, respectively). RNA abundance was normalized to control treatment in each independent experiment; n = 4, *p < 0.04; **p = 0.006, Student's t test (heteroscedastic).
(H) Gene set enrichment analysis of targets common to at least two significantly up-regulated miRNAs.
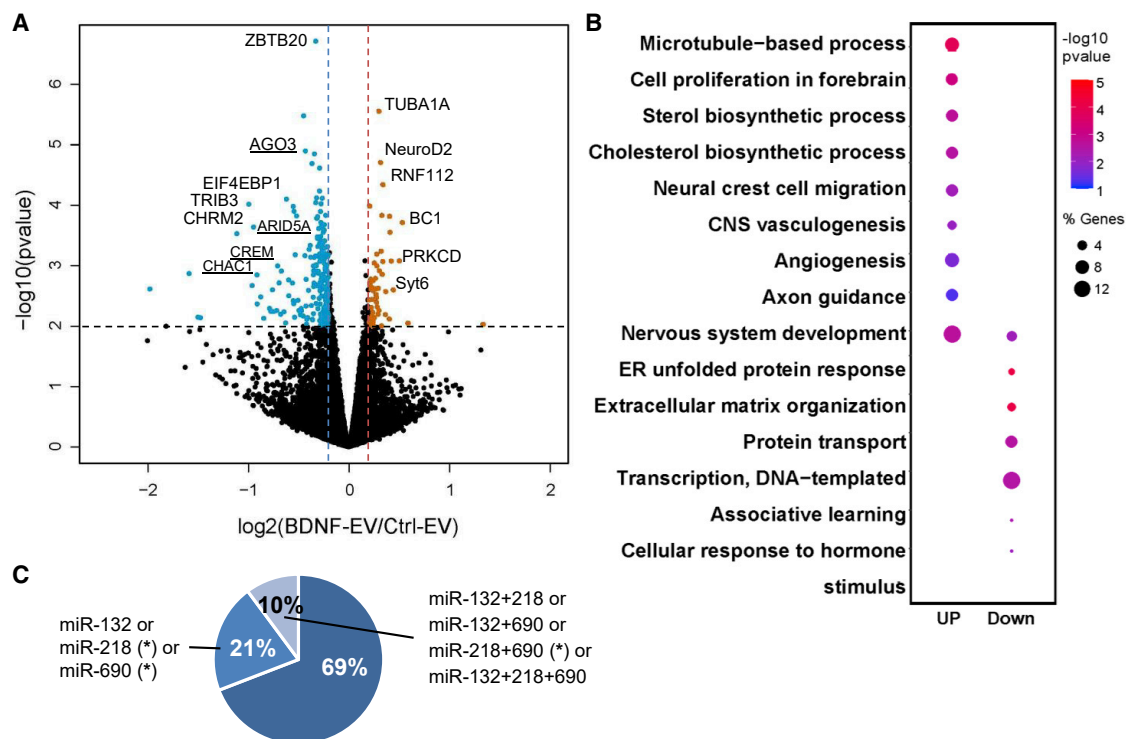See also Figure S3 and Table S1.

**Figure 3. BDNF-EVs differentially regulate gene expression in recipient neurons**

(A) Volcano plot depicting differentially expressed genes in hippocampal neurons treated with Ctrl-EVs or BDNF-EVs for 24 h. Dashed lines reveal fold change and significance thresholds. Up-regulated and down-regulated genes are shown in orange and blue, respectively. Underlined genes are predicted targets of candidate miRNAs; n = 3.

(B) Gene Ontology enrichment of up- or down-regulated genes as shown in (A).

(C) Percentage of genes predicted to be targeted by candidate miRNAs individually or in combination. Asterisks depict significant representation of targets with respect to the mouse genome following hypergeometric testing (*p < 0.005).

See also Figure S4 and Tables S2–S4.

miR-218-5p, with or without miR-690, completely blocked BDNF-induced dendritogenesis compared with miR-Ctrl (Figures 4B, S4C). Importantly, inhibition of all three miRNAs (miR×3 inh) did not decrease BDNF-induced dendrite complexity upon supplementation of neurons with BDNF-EVs (Figures 4C–4E), which is consistent with the functional sEV-mediated delivery of these miRNAs in recipient neurons.

**BDNF-EVs increase excitatory synapse density via regulated miRNAs**

Based on our RNA sequencing and transcriptomics data (Figures 2H and 3), we then examined whether BDNF-EVs and associated miRNAs increase synapse formation. Both BDNF and BDNF-EV treatment significantly increased the overlap between pre- and post-synaptic markers of excitatory synapses PSD95 and synaptophysin (SYP) (Figure 4F) but not between inhibitory synapse markers *vesicular GABA transporter* (vGAT) and gephyrin (Figure S5A), as indicated by Mander's co-localization analysis (Figures 4G and S5B). To investigate whether miR-218-5, miR-132-5, and miR-690 are implicated in BDNF-EV-dependent excitatory synapse maturation, hippocampal neurons were transfected with miR-Ctrl or miR×3 inh, after which neurons were treated with Ctrl or BDNF and immuno-

stained with antibodies against PSD95 and SYP. BDNF treatment significantly increased the number of PSD95-positive spines opposing SYP, which was completely blocked following inhibition of all three miRNAs (Figures 4H, S5C, and S5D). Furthermore, supplementation of neurons with BDNF-EVs, but not Ctrl-EVs, completely rescued this phenotype (Figures 4I and S5E). Importantly, dendritic spine density was not affected in either of these conditions (Figures S5F and S5G). Overall, these data show that sEVs contribute to BDNF-dependent synapse maturation via the inter-neuronal transfer of specific miRNAs.

**SEVs deliver functional miRNAs and are transmitted via synapses**

To verify the transfer of functional miRNA cargo via sEVs, we used a dual fluorescence, bicistronic sensor plasmid for miRNA activity[15] in recipient N2a neuroblastoma cells. The sensor plasmid was designed to contain two miR-218-5p binding sites at the 3′ UTR of dsRed and the EGFP coding sequence under the control of a separate promoter (Figure 5A). N2a cell-derived sEVs decreased the number of dsRed-/GFP-positive recipient cells transfected with the miR-218 sensor ("pSensor") but not control plasmid ("pCtrl") (Figure 5B), which does not contain
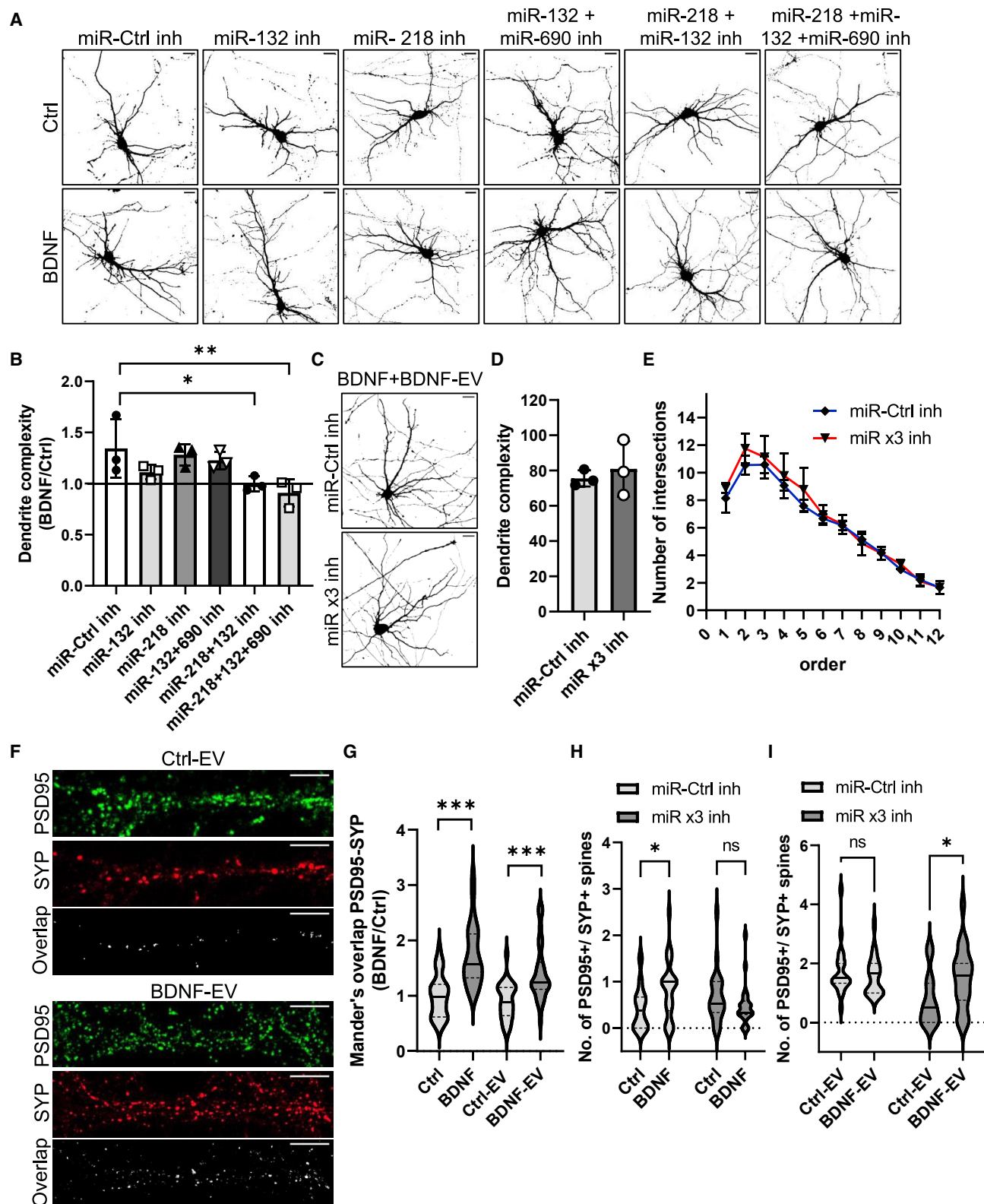
miR-218 binding sites. While repression of the miR-218 sensor was observed in the absence of sEVs, sEV supplementation significantly increased miR-218-dependent sensor repression by approximately 2-fold (2.165% ± 25.9%) (Figures 5B and S6A). To confirm that this effect is not via an indirect increase in miR-218 activity in recipient cells, we transfected recipient cells with miRNA inhibitors against Ctrl (miR-Ctrl) or miR-218-5p prior to addition of sEVs. As expected, inhibition of miR-218-5p in recipient cells increased the basal expression of dsRed in pSensor-expressing, but not pCtrl-expressing, cells, which was significantly reduced upon sEV supplementation (Figures 5C and S6B).

To assess neuronal sEV uptake, we used the high signal-to-noise membrane-binding dye lipilight (also known as MEMbright[38]) to fluorescently label sEVs. Importantly, dye-labeling protocols using fresh cell culture media ("no-cell control") showed a negligible fluorescent signal in recipient neurons when compared with lipilight-labeled sEVs (Figure S6C), confirming the specificity of this dye in EV-labeling experiments. To verify that fluorescent signals are due to sEV internalization, rather than association of sEVs on the cell surface, we treated recipient neurons with the selective dynamin inhibitor dynasore 30 min prior to incubation with sEVs. Little to no lipilight fluorescence was observed in neurons pre-treated with dynasore and either Ctrl-EVs or BDNF-EVs (Figures 5D and 5E), suggesting that the vast majority of neuronal sEVs are taken up via dynamin-dependent endocytosis. Interestingly, inhibition of action potentials in recipient neurons with TTX increased the uptake of lipilight-labeled sEVs (Figures 5F and S6D), suggesting that SV trafficking and sEV uptake may be inter-related. We observed an abundance of membrane emerald GFP (myr-GFP)-EVs at axons of recipient neurons, in close proximity to the SV marker *vesicular glutamate transporter 2* (vGlut2) (Figure S6E). Moreover, we detected the presence of myrGFP-/lipilight-640-double-positive sEVs in the neuritic/axonal compartment of hippocampal neurons seeded in two-part microfluidic chambers (MFCs) (Figure 5G). Here, sEVs were also detected in perisomatic regions 30 min after they were added to the neuritic compartment of fluidically isolated chambers (Figure 5H), suggesting that some sEVs are retrogradely transported to the soma. To further investigate the potential transsynaptic transfer of sEVs, we used three-part MFCs that contained hippocampal neurons in the left and right chambers (1 and 3) but not in the middle (2) chamber. Upon fluidic isolation, chamber 1 and 3 neurons are therefore only linked via synaptic contacts (Figure 5I). Following 24 h incubation in chamber 1, mCherry-CD81 sEVs could be detected in axons in chamber 2 and perisomatic regions of neurons in chamber 3 (Figure 5J). Taken together, these data suggest that sEVs can be taken up at axon terminals and transmitted between neurons via synapses.

## BDNF-induced EVs increase SV clustering

Given the observed pre-synaptic uptake and transsynaptic transfer of EVs (Figures 5F–5J and S6E), we then examined whether BDNF-EVs increase synapse formation by specifically acting on pre-synaptic terminals. Following segmentation, we quantified the density of SYP-positive buttons within 2 $\mu$m from the dendritic surface, as indicated by MAP2 immunostaining (Figure 6A). BDNF-EVs significantly increased the number and mean area of SYP structures (Figures 6B, 6C, and S7A) without affecting mean fluorescence intensity (Figure S7B). Similar results were obtained for the excitatory pre-synaptic marker VGlut2 (Figures S7C–S7E). Moreover, BDNF-EVs isolated from neurons pre-treated with GW4869 did not affect SYP clustering (Figures 6A–6C, S7A, and S7B), suggesting that ceramide-dependent sEVs are important for this phenotype. Importantly, digestion of extraluminal RNA and proteins with RNAse A and trypsin did not affect BDNF-EV-induced clustering of SYP and vGlut (Figures 6D–6F). An increase in the number of MAP2-proximal SYP puncta overlapping with PSD95 was also observed in hippocampal slice cultures incubated with BDNF-EVs, but not Ctrl-EVs, compared with vehicle Ctrl treatment (Figures 6G and S7F). This effect seems to be specific to pre-synaptic terminals as we did not observe an increase in PSD95-positive puncta proximal to MAP2 and SYP (Figure S7G).

To investigate whether BDNF-EVs increase the SV recycling pool, we performed dye uptake experiments using the fixable FM dye analog FM1-43FX. We observed increased FM1-43FX uptake at SYP-positive puncta in proximity to dendrites (SYP-FM) following depolarization with 60 mM KCl (Figures 6H

**Figure 4. BDNF-regulated sEV-miRNAs regulate dendritogenesis and synapse formation**

(A) Hippocampal neurons transfected with dsRed and miRNA inhibitors (inh) against Ctrl miRNA (30 nM) or miR-218, miR-132, and/or miR-690, as depicted (15 or 10 nM each for co-transfection of two or three inhibitors, respectively). Neurons were treated with Ctrl or BDNF and fixed 3 days later (7–10 DIV). Shown are thresholded images based on dsRed fluorescence; scale bars are 20 $\mu$m.

(B) BDNF fold changes in dendrite complexity in neurons as in (A) were quantified using Sholl analysis; n = 3; one-way ANOVA; **p = 0.01; *p = 0.049.

(C) Hippocampal neurons were co-transfected with inhibitors against miR-128-5p, miR-132-5p, and miR-690 ("miR×3 inh") or control ("miR-Ctrl inh") and treated with BDNF as in (A). BDNF-EVs were incubated following BDNF treatment; scale bars are 20 $\mu$m.

(D) Dendrite complexity of neurons treated as in (C) was quantified in Sholl analysis; n = 3.

(E) Sholl profiles of hippocampal neurons treated as in (C). Data are represented as mean ± SEM; n = 3.

(F) Confocal images of neuronal dendrites treated with Ctrl-EVs or BDNF-EVs (7–10 DIV) and immunostained with antibodies against PSD95 and synaptophysin (SYP). Areas of overlap are shown in white; scale bars are 5 $\mu$m.

(G) Quantification of co-localization between PSD95 and SYP. Mander's co-efficients were calculated in dendrite-containing regions of interest in three independent experiments; n = 40, one-way ANOVA, ***p < 0.0001.

(H) Quantification of the number of mature synapses based on the presence of PSD95 and SYP in neurons transfected with miR-Ctrl or miR×3 inh, as in (C), in three independent experiments; n = 30, two-way ANOVA, *p = 0.02.

(I) Quantification of the number of mature synapses in dendrites transfected with miR-Ctrl or miR×3 inh, treated with BDNF and supplemented with either Ctrl-EVs or BDNF-EVs, in three independent experiments; n = 30, two-way ANOVA, *p = 0.02.
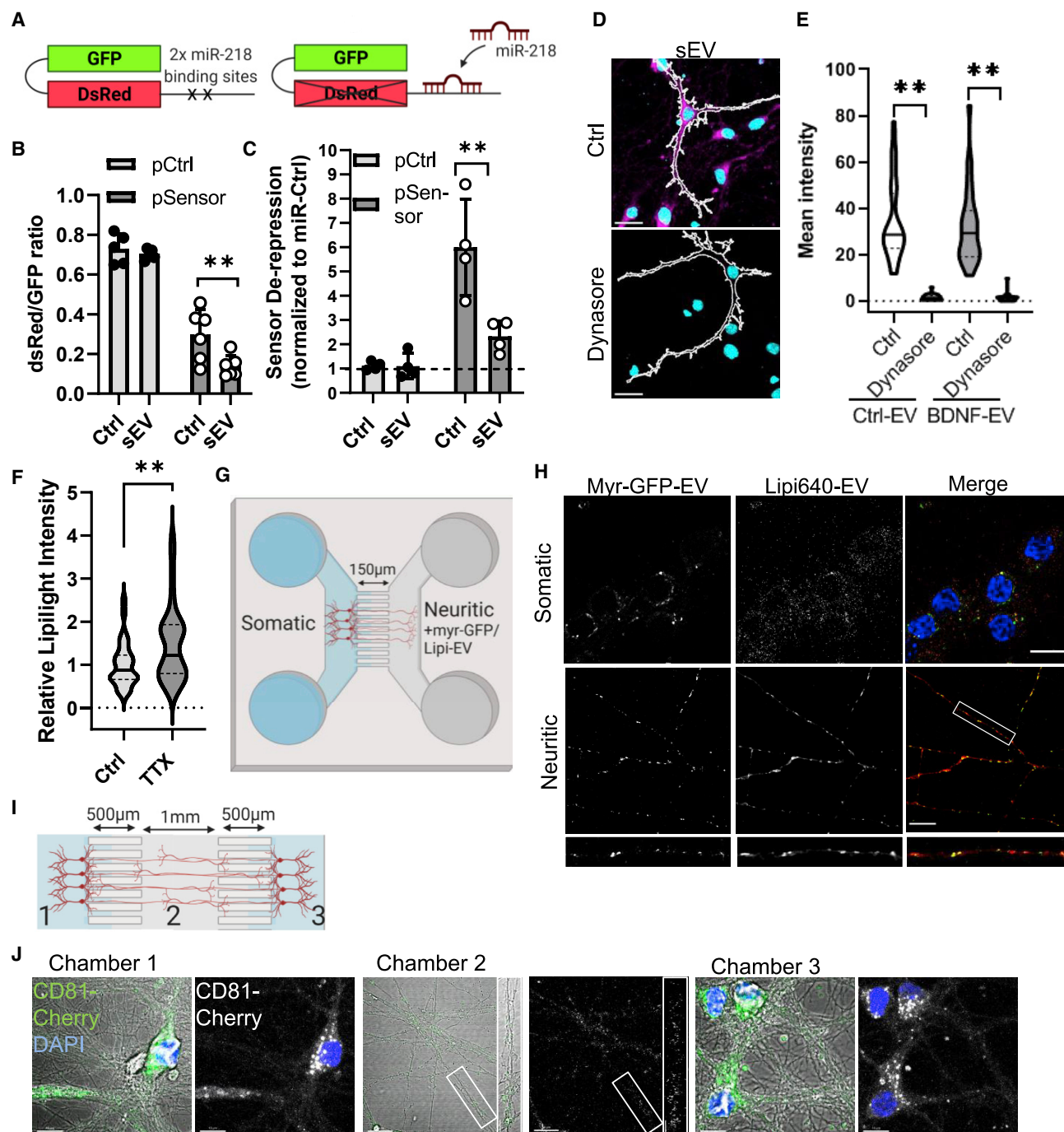
See also Figure S4 and S5.

**Figure 5. sEVs and sEV-miRNAs are taken up by neurons**

(A) Diagram depicting dual-fluorescence sensor for miR-218 activity. Two binding sites for miR-218-5p are present at the 3′ untranslated region (3′ UTR) of dsRed but not GFP.

(B) Quantification of miR-218 activity in N2A cells transfected with the miR-218 sensor as shown in (A) (pSensor) or control plasmid (pCtrl) that does not contain miR-218 binding sites. The number of cells expressing dsRed was counted approximately 20 h following addition of sEVs or control and normalized to the total number of GFP-expressing cells; n = 5–6; *p = 0.002, two-way ANOVA.

(C) Quantification of miR-218 activity in N2A cells transfected with pCtrl or pSensor and miR-218 or Ctrl inhibitor. SEVs were supplemented 1 day after transfection for 22–24 h, and sensor repression was quantified as in (B). Values were normalized to the miR-Ctrl condition in each of four independent experiments; n = 4, two-way ANOVA, *p < 0.01.

(D) Effect of dynasore on sEV uptake. Hippocampal neurons pre-treated with Ctrl or dynasore were incubated with lipilight-560-labeled sEVs for 30 min. White traces mark the outlines of membrane-GFP (mGFP)-expressing hippocampal neurons. Lipilight-560: magenta, DAPI: cyan; scale bars are 20 μm.

*(legend continued on next page)*

and 6I), indicating a bigger SV recycling pool. Consistently, BDNF-EVs increased the mean amplitude of synaptic calcium transients in the presence of TTX (Figures 6J–6L). Overall, these data suggest that BDNF-EVs strengthen synaptic transmission by increasing the functional pool of SVs.

### BDNF-EV-dependent SV clustering is transmissible

Given the observed transsynaptic transport of sEVs between neurons in MFCs (Figure 5J), we wondered whether BDNF-EV-dependent phenotypes may also be observed in second-order neurons, which would indicate that a transmissible phenotype. To this end, we collected sEVs from Ctrl-EV- or BDNF-EV-treated hippocampal neurons ("Ctrl-EV-EVs" and "BDNF-EV-EVs," respectively) and incubated them with naive hippocampal neurons between 7 and 10 DIV (Figure 7A). Remarkably, BDNF-EV-EV-treated neurons had a significantly increased density of both SYP- and vGlut2-positive structures in close proximity to dendrites (Figures 7B–7D). This was not due to soluble factors secreted from Ctrl-EV/BDNF-EV-treated neurons since media depleted from EV-induced EVs (EV-EVs) collected during fractionation did not have an effect on synapse clustering (Figures 7B–7D). Furthermore, EV-EVs were not simply "excess," non-internalized EVs, as these were washed out 4 h after addition to recipient neurons and 16 h prior to collection of EV-EVs (Figure 7A). Therefore, BDNF-EVs induce the sorting and/or secretion of synaptogenesis-promoting sEVs from primary recipient neurons, which may in turn affect network connectivity.

### BDNF-EVs increase neuronal bursting and synchronized activity in hippocampal neurons

To investigate whether BDNF-EVs influence neuronal network activity, extracellular recordings were performed in hippocampal neurons plated in multi-well electrode arrays (MEAs) at 13–14 DIV, when spontaneous neuronal activity typically synchronizes into bursts. Compared with Ctrl-EVs, BDNF-EV-treated neurons had increased neuronal spiking frequency (#p = 0.06) following 24 h incubation (Figures 7E and 7F). This effect was highly specific to synchronous activity, as BDNF-EVs significantly increased the number of spikes per burst and the average burst duration (Figures 7G and 7H). Moreover, BDNF-EV-treated neurons displayed a trend of higher burst frequency within the 20 min recording period (#p = 0.06) (Figure S7H). Interestingly, treatment of hippocampal neurons with BDNF increased the overall number of spikes (Figures 7I and S7I) but did not affect the number of spikes per burst or burst duration (Figures S7J

and S7K). Moreover, GW4869 treatment completely blocked BDNF-induced neuronal firing (Figure 7I), supporting a role for ceramide-dependent sEV secretion in BDNF-dependent neuronal spiking activity. In addition, BDNF increased bursting frequency by 2-fold, which was partially reversed by GW4869 treatment (Figure S7L).

To further assess whether BDNF-EVs influence neuronal connectivity, we performed calcium imaging in hippocampal neuron populations. Calcium traces were extracted from somatic regions of interest (ROIs) (Figure 7J), and Pearson's correlation co-efficients were quantified for each cell in relation to other cells (approximately 60–100 neurons in the field of view). BDNF-EVs increased the overall correlation of calcium traces between neurons (Figures 7K and 7L) without affecting the frequency of calcium events (Figures 7M and S7M). Thus, EVs promote neuronal network connectivity downstream BDNF, which may be important or the establishment and maintenance of neuronal circuits.

### DISCUSSION

We report a mechanism of BDNF-dependent circuit formation via the transsynaptic transfer of sEV-miRNAs. BDNF selectively regulated the sorting of miR-218-5p, miR-132-5p, and miR-690 in neuronal sEVs, which was necessary for the induction of dendrite and synapse maturation. BDNF-EVs selectively increased the clustering of SVs at synapses and promoted synchronous activity in neuronal populations, potentially via the propagation of phenotypes to inter-connected neurons. We propose that sEVs may be important for the long-term establishment of neuronal circuits that may better explain the role of BDNF in neural circuit formation and maintenance.

### Ceramide-dependent sEV biogenesis is necessary for BDNF-EV-induced dendrite and synapse maturation

Several studies have now shown that isolated sEV populations are mainly heterogeneous, likely consisting of sEVs with distinct origins and/or mechanisms of biogenesis.[12] We observed an approximate 1.5-fold reduction of particles in sEV fractions following treatment of donor neurons with GW4869. Based on previous reports in non-neuronal cells,[23–25] this population of sEVs is likely derived from ceramide-dependent formation of intraluminal vesicles in MVEs, although plasma membrane-derived sEVs can so far not be excluded. Interestingly, a ceramide-rich population of sEVs was recently shown to be enriched in RNA in non-neuronal cells.[39] Consistently, GW4869 depleted several miRNAs from sEV fractions without significantly

(E) Lipilight fluorescence intensity was quantified in the somatodendritic compartment of sEV recipient neurons treated as in (D). Shown is the distribution of fluorescence from 10 to 15 neurons per experimental condition; n = 3, two-way ANOVA, **p < 0.02.

(F) Effect of neuronal activity on sEV uptake. Hippocampal neurons were treated with TTX (1 μM; 30 min) prior to the addition of lipilight-560-labeled sEVs (30 min). Fluorescence intensity was normalized to control in three independent experiments; n = 31–32, Student's t test, **p = 0.009.

(G) Schematic of a two-part microfluidic chamber (MFC). Myr-GFP-EVs labeled with lipilight-640 (myr-GFP/Lipi-EVs) were added in the fluidically isolated neuritic compartment for 30 min.

(H) Confocal microscopy images of myr-GFP/Lipi-EVs in the somatic and neuritic compartments of 11 DIV hippocampal neurons treated as in (G). DAPI-stained nuclei are shown in blue; insets represent magnified regions as indicated by the white boxes; scale bars are 20 μm.

(I) Diagram depicting a three-part MFC.

(J) CD81-mCherry-labeled EVs were added to 11 DIV hippocampal neurons in chamber 1 of a three-part MFC following fluidic isolation of all compartments. Neurons were fixed 24 h later. Insets represent magnified regions as indicated by the white boxes; scale bars are 10 μm.
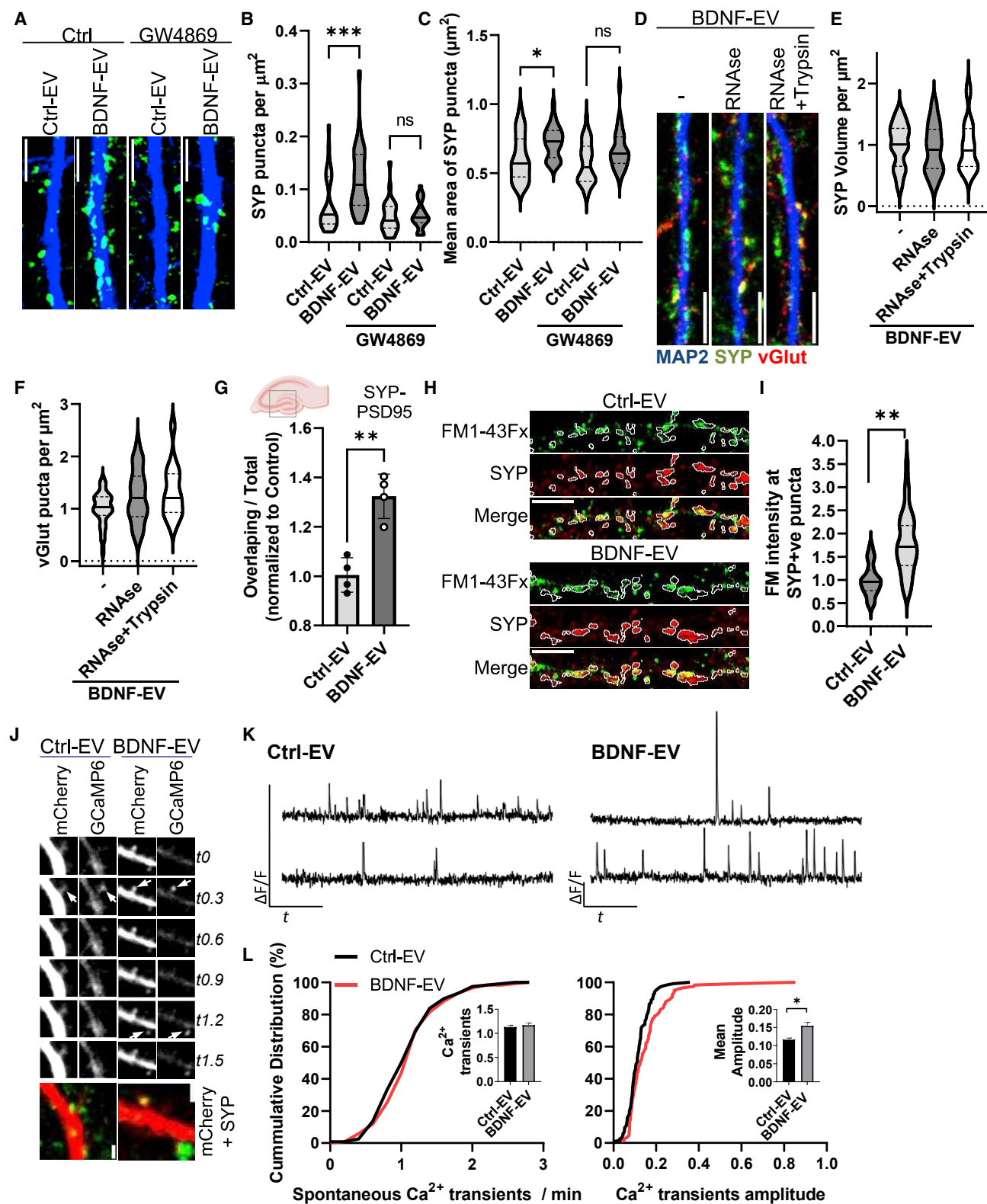
See also Figure S6.

**Figure 6. BDNF-EVs induce excitatory SV clustering in a transmissible manner**

(A) Dendrites of hippocampal neurons incubated with EVs derived from neurons treated with Ctrl or BDNF and GW4869 or control at 7–10 DIV. Recipient neurons were immunostained with anti-SYP (green) and anti-MAP2 (blue) antibodies; scale bar is 5 μm.

*(legend continued on next page)*

affecting their abundance in donor neurons. A notable exception was miR-690, which was not depleted by GW4869, suggesting that this miRNA may be secreted via an alternative biogenesis pathway. Although GW4869 blocked BDNF-EV-induced SV clustering and the BDNF-induced neuronal firing, it did not completely block the BDNF-dependent increase in bursting frequency. As predicted targets of miR-690 were significantly represented in genes down-regulated upon BDNF-EV treatment, we therefore conclude that different types of sEVs may be implicated in this pathway.

### A unique recipe of neuronal BDNF-EV-associated miRNAs to drive complex biological responses

Despite several examples of functional miRNA transfer between cells,[3,40] there is some controversy regarding the efficiency of EV miRNA delivery in recipient cells.[41] Based on our experiments using the dual-fluorescence reporter for miR-218 activity, we argue that this process may become more favorable under certain conditions, depending on the type and state of donor and recipient cells and the availability of mRNA targets in relation to the respective EV-miRNA. In fact, BDNF-EVs increased dendrite complexity in a non-dose-dependent manner, indicating that EV-content delivery can reach a saturation plateau under certain conditions. Notably, more than a third of the genes down-regulated upon BDNF-EV treatment are putative targets of BDNF-EV miRNAs, where targets of miR-218-5p and miR-690 are significantly represented in down-regulated transcripts. This number may be underestimated given that 1) predicted targets were selected on the basis of stringent criteria, 2) other miRNAs present in BDNF-EVs may contribute to sEV-miRNA-mediated translational repression, and 3) local miRNA-dependent changes in translation may not be detectable by whole-cell transcriptomics. As the combined activity of at least two of these miRNAs was necessary for BDNF-dependent dendritogenesis, we suggest that the delivery of a unique miRNA combination may be a characteristic feature of sEV-miRNA-mediated cellular communication. Indeed, the combined activity of specific subsets of intracellular miRNAs was previously shown to be necessary for complex biological responses, such as neuronal differentiation.[42] Accordingly, several mRNA transcripts down-regulated with BDNF-EVs are predicted to be co-targeted by miR-218, miR-132, and/or miR-690 and include regulators of nervous system development, synapse assembly, and axon guidance and transcriptional regulation of gene expression. Notably, miR-132-5p is part of the miR-132/-212 gene cluster that is transcriptionally induced by BDNF[18] and is well-known for its important role in hippocampal plasticity and memory.[43] Moreover, miR-218-5p was previously shown to promote increased synaptic strength[44] and directly regulates the expression of axon guidance molecules such as Slit2,[45] which was down-regulated in BDNF-EV-treated neurons. Interestingly, miR-218 was previously shown to promote resistance to stress-induced depressive behaviors,[46] which are also heavily influenced by BDNF signaling.[47]

### BDNF-EVs as retrograde signaling molecules

BDNF-EVs selectively increased the clustering of excitatory synapse vesicle markers in recipient primary hippocampal neurons and in the dentate gyrus/CA3 regions in hippocampal slices without affecting overall spine density or the number of PSD95-positive post-synaptic terminals. Moreover, we observed the retrograde, transsynaptic transport of fluorescently labeled sEVs in MFCs and the partial overlap between myr-GFP-sEVs and vGlut2-positive SVs, indicating their uptake at pre-synaptic terminals. Interestingly, several miRNAs were shown to regulate local translation in axons, which is thought to be important for rapid structural changes underlying axon guidance.[14,37] As several putative targets of BDNF-EV-associated miRNAs are present in axons and pre-synaptic terminals, our data overall imply the functional delivery of sEV-miRNAs at these sites. This mechanism could enable the fast coupling of pre- and post-synaptic responses via the regulation of translation.

### SEV propagation might tune neuronal circuits downstream BDNF

The notion of EV "spreading" has been previously suggested, particularly in pathological conditions, such as the spreading of toxic aggregates in neurodegenerative diseases,[5,7] during viral infection.[48] Our work provides contextual evidence for a biological role of sEV-mediated propagation between neurons.

(B) The number of SYP-positive structures in proximity to dendrites was quantified in neurons treated as in (A) in three independent experiments; n = 30, one-way ANOVA, **p = 0.001.

(C) The mean area of SYP-positive structures as in (B); n = 30, one-way ANOVA, *p = 0.02.

(D) Representative images of neurons incubated with BDNF-EVs treated with control, RNAse A, or trypsin as depicted; scale bars are 5 μm.

(E) The total volume of SYP-positive structures close to dendrites was quantified in neurons treated as in (D) in three independent experiments; n = 30–31.

(F) Analysis of the number of vGlut-positive structures in proximity to dendrites in neurons processed as in (F); n = 30–31.

(G) BDNF-EV fold changes in the number of SYP-positive puncta overlapping with PSD95 in hippocampal slices. Control vehicle, Ctrl-EVs, or BDNF-EVs, were added to organotypic slices for 3 days. Values were normalized to the total number of SYP puncta and control vehicle; n = 4; Student's t test; *p = 0.001.

(H) Confocal images of SVs labeled with SYP and FM1-43Fx (FM) following treatment with EVs (7–10 DIV). White traces represent re-constructions of SYP fluorescence; scale bar is 5 μm.

(I) Quantification of mean FM fluorescence intensity in SYP-positive structures as in (H). Values were normalized to the Ctrl-EV condition in each of three independent experiments; n = 33–34, Student's t test; **p < 0.0001.

(J) Time-lapse images of dendritic spines in 10–11 DIV neurons transduced with AAV-mCherry and AAV-GCaMP6s, treated with Ctrl- or BDNF-EVs, and imaged in the presence of TTX. Neurons were immunostained with SYP (green, bottom panels) after imaging. Arrows point to increased GCaMP6 fluorescence in dendritic spines; t, time in seconds; scale bars are 2 μm.

(K) Example calcium traces of dendritic spines as in (J).

(L) Cumulative distribution of the number (left) and amplitude (right) of spontaneous calcium transients. Error bars represent standard error of the mean; n = 117–119 regions of interest (ROIs) from 20 cells in three independent experiments; Mann-Whitney test; *p = 0.004.

See also Figure S7.
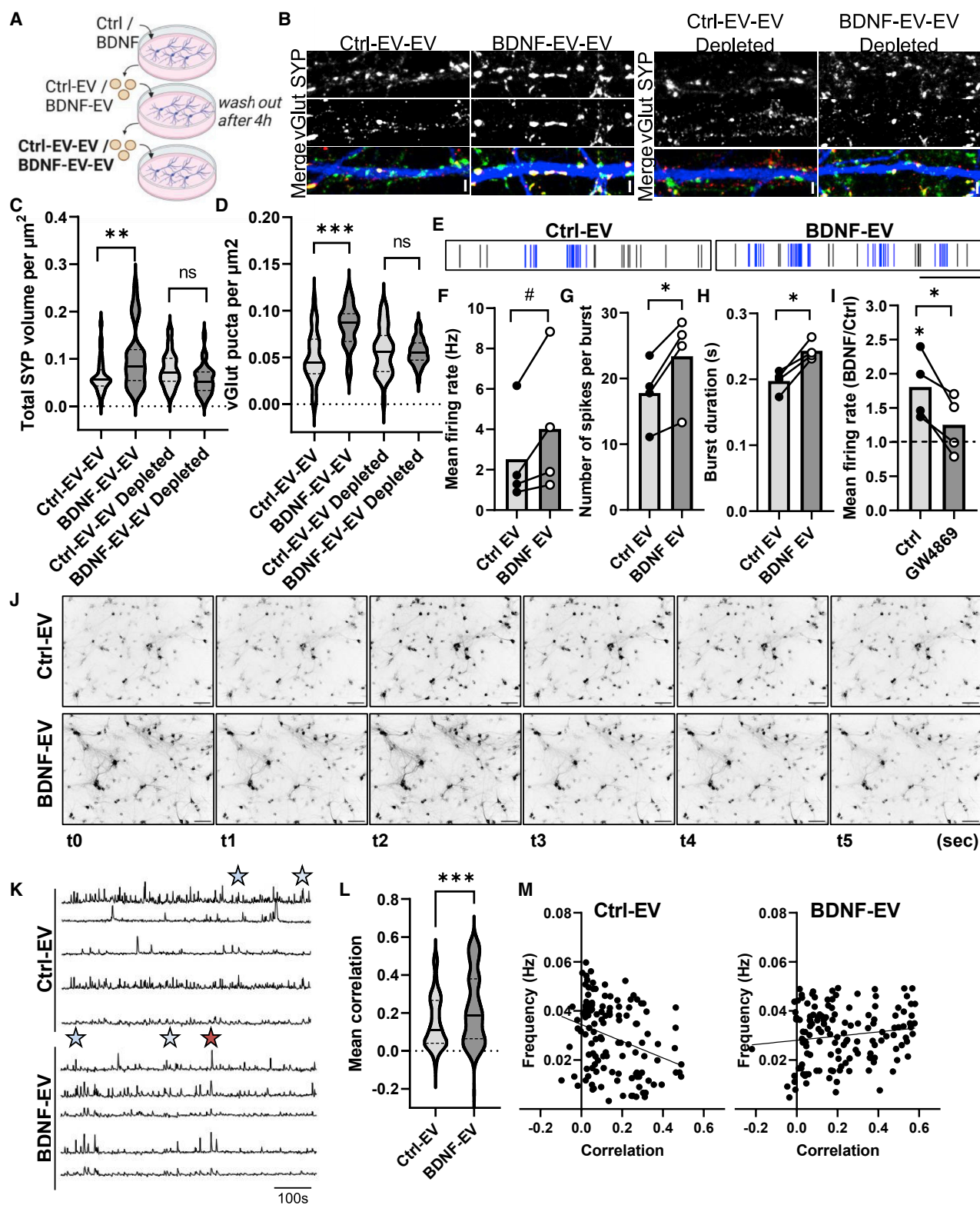
*(legend on next page)*

Although the mechanistic details are so far unclear, we propose three potential ways of EV-phenotype propagation: (1) following miRNA delivery at pre-synaptic terminals, sEVs are retrogradely transported via the endosomal system, potentially re-packaged, and secreted; (2) different subtypes of sEVs either deliver cargo or are further propagated, depending on their surface protein composition, and (3) BDNF-EVs themselves trigger the sorting and secretion of *de novo* EVs that induce synapse formation in secondary neurons.

Given that fluorescent sEVs are not taken up by all neurons in culture, the transsynaptic propagation of BDNF-EV-mediated SV clustering likely underlies the observed increase in synaptic transmission and synchronous neuronal activity. Given the spatial restriction of BDNF-TrkB signaling at specific synapses, this mechanism may further explain, at least in part, the widespread roles of BDNF in neural circuit connectivity.[49–51] We therefore propose that BDNF-induced secretion of sEVs near sites of BDNF-TrkB signaling functions to broadcast synaptic strengthening across populations of inter-connected neurons and thus contributes to the establishment of neuronal networks. Given the relevance of BDNF and BDNF-regulated sEV-miRNAs in neuropsychiatric and mood disorders, this work may ultimately provide a better understanding of the pathophysiology of such diseases.

### Limitations of the study

Although our study addresses the necessity of functional EV cargo miRNA transfer, it does not exclude the involvement of other types of cargo, such as proteins and lipids, as was previously reported in other studies.[10,11] Similar to most studies, we used an excess of EVs for functional experiments. This can be justified given the reported heterogeneity of sEV subtypes.[12,52] Indeed, it was recently shown that only approximately 10% of sEVs are enriched in RNA.[39] To overcome potential misinterpretation of results, we compared BDNF-EVs with Ctrl-EVs, which we argue is a better control than a "non-EV" condition, supported by the observation that BDNF did not affect EV secretion or uptake. However, potential differences in EV processing or cargo delivery in recipient neurons were not investigated. Nonetheless, we did not detect differences in synapse density between non-EV-treated and Ctrl-EV-treated neurons or hippocampal slices, thus supporting the biological relevance of our results. Further investigations of the mechanisms of neuronal EV-miRNA secretion and uptake will undoubtedly be beneficial for understanding their precise roles in the nervous system.

### STAR★METHODS

Detailed methods are provided in the online version of this paper and include the following:

- KEY RESOURCES TABLE
- RESOURCE AVAILABILITY
  - Lead contact
  - Materials availability
  - Data and code availability
- EXPERIMENTAL MODEL AND SUBJECT DETAILS
- METHOD DETAILS
  - Plasmids
  - rAAV production
  - Cell culture
  - Protein analysis
  - EV isolation
  - Nanoparticle tracking analysis (NTA)
  - RNA isolation
  - Whole cell transcriptomics
  - Small RNA sequencing
  - Gene ontology and pathway analysis

**Figure 7. BDNF-EVs induce neuronal bursting activity and synchronized calcium transients**

(A) Diagram depicting experimental workflow for assessment of phenotype spreading. SEVs derived from Ctrl- or BDNF-treated 5–6 DIV cortical neurons were added to 6 DIV hippocampal neurons for 4 h. SEVs from Ctrl-EV- or BDNF-EV-treated neurons (Ctrl-EV-EVs and BDNF-EV-EVs, respectively) were isolated 16 h later and added to 7 DIV naive hippocampal neurons.

(B) Recipient hippocampal neurons treated with Ctrl-EV-EVs, BDNF-EV-EVs, or depleted medium as shown in (A) were immunostained with antibodies against MAP2 (blue), SYP (green), and vGlut2 (red); scale bars are 2 μm.

(C) The volume of SYP in proximity to dendrites treated as in (B) was quantified in three independent experiments; n = 30, one-way ANOVA, **p = 0.005.

(D) The number of vGlut2 puncta in proximity to dendrites treated as in (B) was calculated in three independent experiments; n = 30, one-way ANOVA, ***p < 0.0001.

(E) Representative raster plots of spontaneous neuronal spikes (black) and bursts (blue) in hippocampal neurons plated onto multi-well electrode arrays treated with EVs for 24 h; scale bar is 1 s.

(F) Mean firing rate in neurons treated as in (E); n = 4, Student's t test (heteroscedastic), #p = 0.06.

(G) The number of spikes per burst in neurons treated as in (E); n = 4, Student's t test (heteroscedastic), *p = 0.01.

(H) Burst duration in neurons treated as in (E); n = 4, Student's t test (heteroscedastic), *p = 0.01.

(I) Quantification of men neuronal firing in neurons treated with Ctrl or BDNF (20 min) in the presence or absence of GW4869 or control; n = 4, Student's t test (heteroscedastic), *p < 0.05.

(J) Time lapse images showing calcium activity in 10–11 DIV hippocampal neurons. Shown are thresholded images of the calcium indicator R-GECO1a; scale bars are 20 μm.

(K) Representative somatic calcium traces in neurons treated as in (J). Stars depict regions of synchronized events in all (red) or more than 2 (gray) cells.

(L) The correlation between calcium traces from each neuron in a field of view was quantified using Pearson's correlation analysis in three independent experiments; n = 126–140, Student's t test, ***p = 0.0003.

(M) The mean frequency and correlation of calcium events in Ctrl-EV- and BDNF-EV-treated neurons. Data points represent individual cells. Slopes were analyzed using simple linear regression; Ctrl-EV: n = 126, $R^2$ = 0.1, slope significance from zero, *p = 0.0003; BDNF-EV, n = 140, $R^2$ = 0.02, slope significance from zero, p = 0.09.

See also Figure S7.

- ○ Real-time quantitative PCR (rt-qPCR)
- ○ Immunofluorescence
- ○ Scanning transmission electron microscopy (STEM)
- ○ Image analysis
- ○ Quantification of neuronal activity using multi-electrode arrays (MEA)
- ● QUANTIFICATION AND STATISTICAL ANALYSIS

## REFERENCES

1. van Niel, G., D'Angelo, G., and Raposo, G. (2018). Shedding light on the cell biology of extracellular vesicles. Nat. Rev. Mol. Cell Biol. *19*, 213–228. https://doi.org/10.1038/nrm.2017.125.

2. Mukherjee, C., Kling, T., Russo, B., Miebach, K., Kess, E., Schifferer, M., Pedro, L.D., Weikert, U., Fard, M.K., Kannaiyan, N., et al. (2020). Oligodendrocytes provide antioxidant defense function for neurons by secreting ferritin heavy chain. Cell Metab. *32*, 259–272.e10. https://doi.org/10.1016/j.cmet.2020.05.019.

3. Men, Y., Yelick, J., Jin, S., Tian, Y., Chiang, M.S.R., Higashimori, H., Brown, E., Jarvis, R., and Yang, Y. (2019). Exosome reporter mice reveal the involvement of exosomes in mediating neuron to astroglia communication in the CNS. Nat. Commun. *10*, 4136. https://doi.org/10.1038/s41467-019-11534-w.

4. Bahrini, I., Song, J.h., Diez, D., and Hanayama, R. (2015). Neuronal exosomes facilitate synaptic pruning by up-regulating complement factors in microglia. Sci. Rep. *5*, 7989. https://doi.org/10.1038/srep07989.

5. Wang, Y., Balaji, V., Kaniyappan, S., Krüger, L., Irsen, S., Tepper, K., Chandupatla, R., Maetzler, W., Schneider, A., Mandelkow, E., and Mandelkow, E.M. (2017). The release and trans-synaptic transmission of Tau via exosomes. Mol. Neurodegener. *12*, 5. https://doi.org/10.1186/s13024-016-0143-y.

6. Asai, H., Ikezu, S., Tsunoda, S., Medalla, M., Luebke, J., Haydar, T., Wolozin, B., Butovsky, O., Kügler, S., and Ikezu, T. (2015). Depletion of microglia and inhibition of exosome synthesis halt tau propagation. Nat. Neurosci. *18*, 1584–1593. https://doi.org/10.1038/nn.4132.

7. Sardar Sinha, M., Ansell-Schultz, A., Civitelli, L., Hildesjö, C., Larsson, M., Lannfelt, L., Ingelsson, M., and Hallbeck, M. (2018). Alzheimer's disease pathology propagation by exosomes containing toxic amyloid-beta oligomers. Acta Neuropathol. *136*, 41–56. https://doi.org/10.1007/s00401-018-1868-1.

8. Lim, C.Z.J., Zhang, Y., Chen, Y., Zhao, H., Stephenson, M.C., Ho, N.R.Y., Chen, Y., Chung, J., Reilhac, A., Loh, T.P., et al. (2019). Subtyping of circulating exosome-bound amyloid β reflects brain plaque deposition. Nat. Commun. *10*, 1144. https://doi.org/10.1038/s41467-019-09030-2.

9. Stuendl, A., Kunadt, M., Kruse, N., Bartels, C., Moebius, W., Danzer, K.M., Mollenhauer, B., and Schneider, A. (2016). Induction of α-synuclein aggregate formation by CSF exosomes from patients with Parkinson's disease and dementia with Lewy bodies. Brain *139*, 481–494. https://doi.org/10.1093/brain/awv346.

10. Lee, S.H., Shin, S.M., Zhong, P., Kim, H.-T., Kim, D.-I., Kim, J.M., Heo, W.D., Kim, D.-W., Yeo, C.-Y., Kim, C.-H., and Liu, Q.S. (2018). Reciprocal control of excitatory synapse numbers by Wnt and Wnt inhibitor PRR7 secreted on exosomes. Nat. Commun. *9*, 3434. https://doi.org/10.1038/s41467-018-05858-2.

11. Vilcaes, A.A., Chanaday, N.L., and Kavalali, E.T. (2021). Interneuronal exchange and functional integration of synaptobrevin via extracellular vesicles. Neuron *109*, 971–983.e5. https://doi.org/10.1016/j.neuron.2021.01.007.

12. Jeppesen, D.K., Fenix, A.M., Franklin, J.L., Higginbotham, J.N., Zhang, Q., Zimmerman, L.J., Liebler, D.C., Ping, J., Liu, Q., Evans, R., et al. (2019). Reassessment of exosome composition. Cell *177*, 428–445.e18. https://doi.org/10.1016/j.cell.2019.02.029.

13. Sambandan, S., Akbalik, G., Kochen, L., Rinne, J., Kahlstatt, J., Glock, C., Tushev, G., Alvarez-Castelao, B., Heckel, A., and Schuman, E.M. (2017). Activity-dependent spatially localized miRNA maturation in neuronal dendrites. Science *355*, 634–637. https://doi.org/10.1126/science.aaf8995.

14. Corradi, E., Dalla Costa, I., Gavoci, A., Iyer, A., Roccuzzo, M., Otto, T.A., Oliani, E., Bridi, S., Strohbuecker, S., Santos-Rodriguez, G., et al. (2020). Axonal precursor miRNAs hitchhike on endosomes and locally regulate the development of neural circuits. EMBO J. *39*, e102513. https://doi.org/10.15252/embj.2019102513.

15. Antoniou, A., Khudayberdiev, S., Idziak, A., Bicker, S., Jacob, R., and Schratt, G. (2018). The dynamic recruitment of TRBP to neuronal membranes mediates dendritogenesis during development. EMBO Rep. *19*, e44853. https://doi.org/10.15252/embr.201744853.

16. Rajman, M., and Schratt, G. (2017). MicroRNAs in neural development: from master regulators to fine-tuners. Development *144*, 2310–2322. https://doi.org/10.1242/dev.144337.

17. Huang, Y.-W.A., Ruiz, C.R., Eyler, E.C.H., Lin, K., and Meffert, M.K. (2012). Dual regulation of miRNA biogenesis generates target specificity in neurotrophin-induced protein synthesis. Cell *148*, 933–946. https://doi.org/10.1016/j.cell.2012.01.036.

18. Vo, N., Klein, M.E., Varlamova, O., Keller, D.M., Yamamoto, T., Goodman, R.H., and Impey, S. (2005). A cAMP-response element binding protein-induced microRNA regulates neuronal morphogenesis. Proc. Natl. Acad. Sci. USA *102*, 16426–16431. https://doi.org/10.1073/pnas.0508448102.

19. Antoniou, A., Baptista, M., Carney, N., and Hanley, J.G. (2014). PICK1 links Argonaute 2 to endosomes in neuronal dendrites and regulates miRNA activity. EMBO Rep. *15*, 548–556. https://doi.org/10.1002/embr.201337631.

20. Wang, C.S., Kavalali, E.T., and Monteggia, L.M. (2022). BDNF signaling in context: from synaptic regulation to psychiatric disorders. Cell *185*, 62–76. https://doi.org/10.1016/j.cell.2021.12.003.

21. Horch, H.W., and Katz, L.C. (2002). BDNF release from single cells elicits local dendritic growth in nearby neurons. Nat. Neurosci. *5*, 1177–1184. https://doi.org/10.1038/nn927.

22. Martins, H.C., and Schratt, G. (2021). MicroRNA-dependent control of neuroplasticity in affective disorders. Transl. Psychiatry *11*, 263. https://doi.org/10.1038/s41398-021-01379-7.

23. Catalano, M., and O'Driscoll, L. (2020). Inhibiting extracellular vesicles formation and release: a review of EV inhibitors. J. Extracell. Vesicles *9*, 1703244. https://doi.org/10.1080/20013078.2019.1703244.

24. Trajkovic, K., Hsu, C., Chiantia, S., Rajendran, L., Wenzel, D., Wieland, F., Schwille, P., Brügger, B., and Simons, M. (2008). Ceramide triggers budding of exosome vesicles into multivesicular endosomes. Science *319*, 1244–1247. https://doi.org/10.1126/science.1153124.

25. Menck, K., Sönmezer, C., Worst, T.S., Schulz, M., Dihazi, G.H., Streit, F., Erdmann, G., Kling, S., Boutros, M., Binder, C., and Gross, J.C. (2017). Neutral sphingomyelinases control extracellular vesicles budding from the plasma membrane. J. Extracell. Vesicles *6*, 1378056. https://doi.org/10.1080/20013078.2017.1378056.

26. Lachenal, G., Pernet-Gallay, K., Chivet, M., Hemming, F.J., Belly, A., Bodon, G., Blot, B., Haase, G., Goldberg, Y., and Sadoul, R. (2011). Release of exosomes from differentiated neurons and its regulation by synaptic glutamatergic activity. Mol. Cell. Neurosci. *46*, 409–418. https://doi.org/10.1016/j.mcn.2010.11.004.

27. Ying, S.-W., Futter, M., Rosenblum, K., Webber, M.J., Hunt, S.P., Bliss, T.V.P., and Bramham, C.R. (2002). Brain-derived neurotrophic factor induces long-term potentiation in intact adult hippocampus: requirement for ERK activation coupled to CREB and upregulation of Arc synthesis. J. Neurosci. *22*, 1532–1540. https://doi.org/10.1523/JNEUROSCI.22-05-01532.2002.

28. Fiore, R., Khudayberdiev, S., Christensen, M., Siegel, G., Flavell, S.W., Kim, T.-K., Greenberg, M.E., and Schratt, G. (2009). Mef2-mediated transcription of the miR379-410 cluster regulates activity-dependent dendritogenesis by fine-tuning Pumilio2 protein levels. EMBO J. *28*, 697–710. https://doi.org/10.1038/emboj.2009.10.

29. Arroyo, J.D., Chevillet, J.R., Kroh, E.M., Ruf, I.K., Pritchard, C.C., Gibson, D.F., Mitchell, P.S., Bennett, C.F., Pogosova-Agadjanyan, E.L., Stirewalt, D.L., et al. (2011). Argonaute2 complexes carry a population of circulating microRNAs independent of vesicles in human plasma. Proc. Natl. Acad. Sci. USA *108*, 5003–5008. https://doi.org/10.1073/pnas.1019055108.

30. McDermott, J.E., Goldblatt, D., and Paradis, S. (2018). Class 4 Semaphorins and Plexin-B receptors regulate GABAergic and glutamatergic synapse development in the mammalian hippocampus. Mol. Cell. Neurosci. *92*, 50–66. https://doi.org/10.1016/j.mcn.2018.06.008.

31. Jongbloets, B.C., Lemstra, S., Schellino, R., Broekhoven, M.H., Parkash, J., Hellemons, A.J.C.G.M., Mao, T., Giacobini, P., van Praag, H., De Marchis, S., et al. (2017). Stage-specific functions of Semaphorin7A during adult hippocampal neurogenesis rely on distinct receptors. Nat. Commun. *8*, 14666. https://doi.org/10.1038/ncomms14666.

32. Suto, F., Tsuboi, M., Kamiya, H., Mizuno, H., Kiyama, Y., Komai, S., Shimizu, M., Sanbo, M., Yagi, T., Hiromi, Y., et al. (2007). Interactions between plexin-A2, plexin-A4, and semaphorin 6A control lamina-restricted projection of hippocampal mossy fibers. Neuron *53*, 535–547. https://doi.org/10.1016/j.neuron.2007.01.028.

33. Teo, S., and Salinas, P.C. (2021). Wnt-frizzled signaling regulates activity-mediated synapse formation. Front. Mol. Neurosci. *14*, 683035. https://doi.org/10.3389/fnmol.2021.683035.

34. Ince-Dunn, G., Hall, B.J., Hu, S.-C., Ripley, B., Huganir, R.L., Olson, J.M., Tapscott, S.J., and Ghosh, A. (2006). Regulation of thalamocortical patterning and synaptic maturation by NeuroD2. Neuron *49*, 683–695. https://doi.org/10.1016/j.neuron.2006.01.031.

35. Aguado, F., Díaz-Ruiz, C., Parlato, R., Martínez, A., Carmona, M.A., Bleckmann, S., Ureña, J.M., Burgaya, F., del Río, J.A., Schütz, G., and Soriano, E. (2009). The CREB/CREM transcription factors negatively regulate early synaptogenesis and spontaneous network activity. J. Neurosci. *29*, 328–333. https://doi.org/10.1523/JNEUROSCI.5252-08.2009.

36. Duan, Y., Wang, S.-H., Song, J., Mironova, Y., Ming, G.l., Kolodkin, A.L., and Giger, R.J. (2014). Semaphorin 5A inhibits synaptogenesis in early postnatal- and adult-born hippocampal dentate granule cells. Elife *3*, e04390. https://doi.org/10.7554/eLife.04390.

37. Bellon, A., Iyer, A., Bridi, S., Lee, F.C.Y., Ovando-Vázquez, C., Corradi, E., Longhi, S., Roccuzzo, M., Strohbuecker, S., Naik, S., et al. (2017). miR-182 regulates slit2-mediated axon guidance by modulating the local translation of a specific mRNA. Cell Rep. *18*, 1171–1186. https://doi.org/10.1016/j.celrep.2016.12.093.

38. Collot, M., Ashokkumar, P., Anton, H., Boutant, E., Faklaris, O., Galli, T., Mély, Y., Danglot, L., and Klymchenko, A.S. (2019). Membright: a family of fluorescent membrane probes for advanced cellular imaging and neuroscience. Cell Chem. Biol. *26*, 600–614.e7. https://doi.org/10.1016/j.chembiol.2019.01.009.

39. Barman, B., Sung, B.H., Krystofiak, E., Ping, J., Ramirez, M., Millis, B., Allen, R., Prasad, N., Chetyrkin, S., Calcutt, M.W., et al. (2022). VAP-A and its binding partner CERT drive biogenesis of RNA-containing extracellular vesicles at ER membrane contact sites. Dev. Cell *57*, 974–994.e8. https://doi.org/10.1016/j.devcel.2022.03.012.

40. Xu, B., Zhang, Y., Du, X.-F., Li, J., Zi, H.-X., Bu, J.-W., Yan, Y., Han, H., and Du, J.-L. (2017). Neurons secrete miR-132-containing exosomes to regulate brain vascular integrity. Cell Res. *27*, 882–897. https://doi.org/10.1038/cr.2017.62.

41. Chevillet, J.R., Kang, Q., Ruf, I.K., Briggs, H.A., Vojtech, L.N., Hughes, S.M., Cheng, H.H., Arroyo, J.D., Meredith, E.K., Gallichotte, E.N., et al. (2014). Quantitative and stoichiometric analysis of the microRNA content of exosomes. Proc. Natl. Acad. Sci. USA *111*, 14888–14893. https://doi.org/10.1073/pnas.1408301111.

42. Pons-Espinal, M., de Luca, E., Marzi, M.J., Beckervordersandforth, R., Armirotti, A., Nicassio, F., Fabel, K., Kempermann, G., and De Pietri Tonelli, D. (2017). Synergic functions of miRNAs determine neuronal fate of adult neural stem cells. Stem Cell Rep. *8*, 1046–1061. https://doi.org/10.1016/j.stemcr.2017.02.012.

43. Aten, S., Hansen, K.F., Hoyt, K.R., and Obrietan, K. (2016). The miR-132/212 locus: a complex regulator of neuronal plasticity, gene expression and cognition. RNA Dis. *3*, e1375. https://doi.org/10.14800/rd.1375.

44. Rocchi, A., Moretti, D., Lignani, G., Colombo, E., Scholz-Starke, J., Baldelli, P., Tkatch, T., and Benfenati, F. (2019). Neurite-enriched MicroRNA-218 stimulates translation of the GluA2 subunit and increases excitatory synaptic strength. Mol. Neurobiol. *56*, 5701–5714. https://doi.org/10.1007/s12035-019-1492-7.

45. Small, E.M., Sutherland, L.B., Rajagopalan, K.N., Wang, S., and Olson, E.N. (2010). MicroRNA-218 regulates vascular patterning by modulation of Slit-Robo signaling. Circ. Res. *107*, 1336–1344. https://doi.org/10.1161/CIRCRESAHA.110.227926.

46. Torres-Berrío, A., Nouel, D., Cuesta, S., Parise, E.M., Restrepo-Lozano, J.M., Larochelle, P., Nestler, E.J., and Flores, C. (2020). MiR-218: a molecular switch and potential biomarker of susceptibility to stress. Mol. Psychiatry *25*, 951–964. https://doi.org/10.1038/s41380-019-0421-5.

47. Notaras, M., and van den Buuse, M. (2020). Neurobiology of BDNF in fear memory, sensitivity to stress, and stress-related disorders. Mol. Psychiatry *25*, 2251–2274. https://doi.org/10.1038/s41380-019-0639-2.

48. Nolte-'t Hoen, E., Cremer, T., Gallo, R.C., and Margolis, L.B. (2016). Extracellular vesicles and viruses: are they close relatives? Proc. Natl. Acad. Sci. USA *113*, 9155–9161. https://doi.org/10.1073/pnas.1605146113.

49. Niculescu, D., Michaelsen-Preusse, K., Güner, Ü., van Dorland, R., Wierenga, C.J., and Lohmann, C. (2018). A BDNF-mediated push-pull plasticity mechanism for synaptic clustering. Cell Rep. *24*, 2063–2074. https://doi.org/10.1016/j.celrep.2018.07.073.

50. Staras, K., Branco, T., Burden, J.J., Pozo, K., Darcy, K., Marra, V., Ratnayaka, A., and Goda, Y. (2010). A vesicle superpool spans multiple presynaptic terminals in hippocampal neurons. Neuron *66*, 37–44. https://doi.org/10.1016/j.neuron.2010.03.020.

51. Bamji, S.X., Rico, B., Kimes, N., and Reichardt, L.F. (2006). BDNF mobilizes synaptic vesicles and enhances synapse formation by disrupting cadherin-beta-catenin interactions. J. Cell Biol. *174*, 289–299. https://doi.org/10.1083/jcb.200601087.

52. Kowal, J., Arras, G., Colombo, M., Jouve, M., Morath, J.P., Primdal-Bengtson, B., Dingli, F., Loew, D., Tkach, M., and Théry, C. (2016). Proteomic comparison defines novel markers to characterize heterogeneous populations of extracellular vesicle subtypes. Proc. Natl. Acad. Sci. USA *113*, E968–E977. https://doi.org/10.1073/pnas.1521230113.

53. Chen, T.-W., Wardill, T.J., Sun, Y., Pulver, S.R., Renninger, S.L., Baohan, A., Schreiter, E.R., Kerr, R.A., Orger, M.B., Jayaraman, V., et al. (2013). Ultrasensitive fluorescent proteins for imaging neuronal activity. Nature *499*, 295–300. https://doi.org/10.1038/nature12354.

54. Dana, H., Mohar, B., Sun, Y., Narayan, S., Gordus, A., Hasseman, J.P., Tsegaye, G., Holt, G.T., Hu, A., Walpita, D., et al. (2016). Sensitive red protein calcium indicators for imaging neural activity. Elife *5*, e12727. https://doi.org/10.7554/eLife.12727.

55. Kügler, S., Lingor, P., Schöll, U., Zolotukhin, S., and Bähr, M. (2003). Differential transgene expression in brain cells in vivo and in vitro from AAV-2 vectors with small transcriptional control units. Virology *311*, 89–95. https://doi.org/10.1016/S0042-6822(03)00162-4.

56. Schindelin, J., Arganda-Carreras, I., Frise, E., Kaynig, V., Longair, M., Pietzsch, T., Preibisch, S., Rueden, C., Saalfeld, S., Schmid, B., et al. (2012). Fiji: an open-source platform for biological-image analysis. Nat. Methods *9*, 676–682. https://doi.org/10.1038/nmeth.2019.

57. Van Rossum, G., and Drake, F.L. (2009). Python 3 Reference Manual: (Python Documentation Manual Part 2) (CreateSpace Independent Publishing Platform)).

58. Risso, D., Ngai, J., Speed, T.P., and Dudoit, S. (2014). Normalization of RNA-seq data using factor analysis of control genes or samples. Nat. Biotechnol. *32*, 896–902. https://doi.org/10.1038/nbt.2931.

59. Somiya, M., and Kuroda, S. (2020). Real-time luminescence assay for cytoplasmic cargo delivery of extracellular vesicles. Preprint at bioRxiv. https://doi.org/10.1101/2020.10.16.341974.

60. Christensen, M., Larsen, L.A., Kauppinen, S., and Schratt, G. (2010). Recombinant adeno-associated virus-mediated microRNA delivery into the postnatal mouse brain reveals a role for miR-134 in dendritogenesis in vivo. Front. Neural Circuits *3*, 16. https://doi.org/10.3389/neuro.04.016.2009.

61. De Simoni, A., and Yu, L.M.Y. (2006). Preparation of organotypic hippocampal slice cultures: interface method. Nat. Protoc. *1*, 1439–1445. https://doi.org/10.1038/nprot.2006.228.

62. Théry, C., Witwer, K.W., Aikawa, E., Alcaraz, M.J., Anderson, J.D., Andriantsitohaina, R., Antoniou, A., Arab, T., Archer, F., Atkin-Smith, G.K., et al. (2018). Minimal information for studies of extracellular vesicles 2018 (MISEV2018): a position statement of the International Society for Extracellular Vesicles and update of the MISEV2014 guidelines. J. Extracell. Vesicles *7*, 1535750. https://doi.org/10.1080/20013078.2018.1535750.

63. Dweep, H., Sticht, C., Pandey, P., and Gretz, N. (2011). miRWalk–database: prediction of possible miRNA binding sites by "walking" the genes of three genomes. J. Biomed. Inform. *44*, 839–847. https://doi.org/10.1016/j.jbi.2011.05.002.

64. Dweep, H., and Gretz, N. (2015). miRWalk2.0: a comprehensive atlas of microRNA-target interactions. Nat. Methods *12*, 697. https://doi.org/10.1038/nmeth.3485.

65. Huang, D.W., Sherman, B.T., and Lempicki, R.A. (2009). Systematic and integrative analysis of large gene lists using DAVID bioinformatics resources. Nat. Protoc. *4*, 44–57. https://doi.org/10.1038/nprot.2008.211.

66. Huang, D.W., Sherman, B.T., and Lempicki, R.A. (2009). Bioinformatics enrichment tools: paths toward the comprehensive functional analysis of large gene lists. Nucleic Acids Res. *37*, 1–13. https://doi.org/10.1093/nar/gkn923.

## STAR★METHODS

### KEY RESOURCES TABLE

| REAGENT or RESOURCE | SOURCE | IDENTIFIER |
| --- | --- | --- |
| **Antibodies** | | |
| Actin | Sigma-Aldrich | Cat#A4700 |
| AKT | Cell Signaling | Cat#4685 |
| Alix | GeneTex | Cat#GTX42812 |
| BDNF | Abcam | Cat#ab108319 |
| Biotin | Life Technologies | Cat#S32354 |
| Calnexin | Abcam | Cat#ab2301 |
| ERK1/2 (p44/42 MAPK) | Cell Signaling | Cat#9102 |
| Flotilin-2 | Santa Cruz | Cat#sc-25507 |
| GABA | Sigma-Aldrich | Cat#A2052 |
| Gephyrin | Cell Signaling | Cat#43928 |
| GFAP | Synaptic Systems | Cat#173004 |
| Grp75 | Abcam | Cat#ab53098 |
| Lamp1 | Abcam | Cat#ab24170 |
| MAP2 | Abcam | Cat#ab11268 |
| MAP2 | Abcam | Cat#ab5392 |
| Myc | Cell Signaling | Cat#2276 |
| N-Cadherin | BD Biosciences | Cat#610920 |
| Phospho-AKT (Ser473) | Cell Signaling | Cat#9271 |
| Phospho-ERK1/2 (Thr202/Tyr204) | Cell Signaling | Cat#4370 |
| Phospho-TrkB (Tyr816) | Merckmillipore | Cat#ABN1381 |
| PSD95 | Merckmillipore | Cat#MAB1596 |
| PSD95 | ThermoScientific | Cat#MA1-0416 |
| Synaptophysin | Abcam | Cat#ab16659 |
| TrkB | RnD Systems | Cat#AF1494 |
| TSG101 | Santa Cruz | Cat#sc-7964 |
| vGAT | ThermoScientific | Cat#MA5-24643 |
| VGlut2 | Synaptic Systems | Cat#135404 |
| **Bacterial and virus strains** | | |
| pAAV1-Syn-GCaMP6s-WPRE-SV40 | Chen et al.[53] | Addgene#100843 |
| pAAV1-Syn-NES-jRGECO1a-WPRE-SV40 | Dana et al.[54] | Addgene#100854 |
| SURE2 Supercompetent Cells | Agilent | Cat#200152 |
| pAAV2/6-Syn-mCherry | This paper | N/A |
| pAAV2/6-Syn-mCherry-CD81 | This paper | N/A |
| pAAV2/6-Syn-myr-emGFP | This paper | N/A |
| **Chemicals, peptides, and recombinant proteins** | | |
| AraC | Sigma-Aldrich | Cat#C6645 CAS 69-74-9 |
| Bicuculline Methiodide | Sigma-Aldrich | Cat#14343 CAS 40709-69-1 |
| CNQX | Tocris | Cat#1045 CAS 479347-85-8 |
| D-APV | Tocris | Cat#0106 CAS 79055-68-8 |
| Dynasore Hydrate | Sigma-Aldrich | Cat#D7693 CAS; 1202867-00-2 |
| FM1-43Fx | Thermo Fisher | Cat#F35355 |
| GW4869 | Sigma-Aldrich | Cat#D1692 CAS 6823-69-4 |
| Lipilight | Collot et al.[38] | N/A |

*(Continued on next page)*

*Continued*

| REAGENT or RESOURCE | SOURCE | IDENTIFIER |
|---|---|---|
| Recombinant BDNF | Peprotech | Cat#450–02 |
| Recombinant myc | Chromotek | N/A |
| Recombinant myc-BDNF | Cusabio | N/A |
| Tetrodotoxin | Biozol | Cat#HLB-HB1035 CAS: 18660-81-6 |
| U0126 | MerckMillipore | Cat#662005 CAS 109511-58-2 |
| **Critical commercial assays** | | |
| miRNeasy micro kit | Qiagen | Cat#217084 |
| NEBNext Multiplex Small RNA Library Prep Set for Illumina | New England Biolabs | Cat#E7300, E7580, E7560 |
| QubitTM dsDNA HS Assay Kit | Thermo Fisher | Cat#Q32851 |
| TaqMan Advanced miRNA cDNA synthesis kit | Thermo Fisher | Cat#A28007 |
| TaqMan Fast Advanced Master Mix | Thermo Fisher | Cat#4444557 |
| TruSeq RNA library prep kit v2 | Illumina | Cat#RS-122-2001 |
| **Deposited data** | | |
| Raw and analyzed data | This paper | GEO Accession: GSE184945 |
| **Experimental models: Organisms/strains** | | |
| Mouse: NMRI | Charles River Laboratories | Strain Code: 605 |
| **Oligonucleotides** | | |
| mmu-miR-132-5p | Thermo Fisher | Cat# A25576 Assay ID:mmu481539_mir |
| mmu-miR-218-5p | Thermo Fisher | Cat# A25576 Assay ID: mmu481001_mir |
| mmu-miR-690 | Thermo Fisher | Cat# A25576 Assay ID: mmu482837_mir |
| mmu-miR-181a-5p | Thermo Fisher | Cat# A25576 Assay ID: mmu481485_mir |
| mmu-miR-129-2-3p | Thermo Fisher | Cat# A25576 Assay ID: mmu478544_mir |
| mmu-miR-218-5p | Thermo Fisher | Cat# 4464066 Assay ID: MC10328 |
| mmu-miR-132-5p | Thermo Fisher | Cat# 4464084 Assay ID: MH19230 |
| mmu-miR-218-5p | Thermo Fisher | Cat# 4464084 Assay ID:MH10328 |
| mmu-miR-690 | Thermo Fisher | Cat# 4464084 Assay ID: MH11517 |
| See Table S5 for additional oligonucleotides including primers for cloning, Arc and GAPDH | | |
| **Recombinant DNA** | | |
| pAAV-6p-SEWB-hSyn-GFP | Kugler et al.[55] | N/A |
| pAAV-6p-SEWB-hSyn-myr-emGFP | This paper | N/A |
| pAAV-hSyn-mCherry-CD81 | This paper | N/A |
| pAAV-hSyn-mCherry | This paper | N/A |
| pTracer-CMV-dsRed | Fiore et al.[28] | N/A |
| pTracer-miR218-dsRed-GFP | This paper | N/A |
| **Software and algorithms** | | |
| Fiji | Schindelin et al.[56] | https://www.fiji.sc |
| Imaris9.7 | Oxford Instruments | https://imaris.oxinst.com |
| Python version 3 | Python Software Foundation[57] | https://www.python.org |
| R | RStudio Team (2020). RStudio: Integrated Development for R. RStudio, PBC, Boston, MA URL | https://www.posit.co |
| RUVSeq package1 | Risso et al.[58] | https://www.bioconductor.org |

## RESOURCE AVAILABILITY

### Lead contact
Further information and requests for resources and reagents should be directed to and will be fulfilled by the lead contact Anja Schneider (anja.schneider@dzne.de).

**Materials availability**

This study did not generate any new reagents.

**Data and code availability**

- RNA sequencing data have been deposited at GEO and are publically available as of the date of publication. Accession numbers are listed in the key resources table. Primary data reported in this study will be shared by the lead contact upon request.
- This paper does not report original code.
- Any additional information required to reanalyze the data in this paper is available from the lead contact upon request.

## EXPERIMENTAL MODEL AND SUBJECT DETAILS

Primary cortical and hippocampal neurons were derived from male and female NMRI mice at embryonic day 16 (E16) according to Animal Welfare regulations. Primary neurons were maintained in MEM-B27 medium and kept in a humidified incubator supplied with 5% $CO_2$ at 37°C. N2A neuroblastoma and HEK293T cells were maintained in DMEM supplemented with 10% fetal bovine serum (FBS) in a humidified incubator with 5% $CO_2$ at 37°C. Cells were not used after 25 passages and each batch was tested for mycoplasma contamination by PCR.

## METHOD DETAILS

### Plasmids

Plasmids for dsRed and dual fluorescence miRNA sensors were used as previously described.[15] Plasmids for rAAV production pAAV-6p-SEWB-hSyn-GFP and PDP6 were kindly provided by Sebastian Kuegler.[55] For production of membrane emGFP (myr-GFP), a myristoylation sequence was cloned upstream emerald GFP and sub-cloned into pAAV plasmid downstream the human Synapsin 1 promoter. pCA-HiBiT-CD81 was a gift from Masaharu Somiya (Addgene plasmid #162593)[59] and was used to construct pAAV-hSyn-mCherry-CD81. Custom primers were purchased from Sigma and miRNA probes were from Life Technologies.

### rAAV production

Sub-confluent Hek293T cells were co-transfected with equimolar concentrations of pAAV-6p-hSyn-myr-GFP, pAAV-6p-hSyn-Cherry or pAAV-6p-hSyn-mCherry-CD81 and pDP6 helper plasmid using the calcium phosphate method with a final $CaCl_2$ concentration of 0.1M. Crude lysates were prepared 2–3 days later by re-suspending cells in 150mM NaCl, 20mM Tris pH8 and freeze-thawing following treatment with a final concentration of 50U/mL benzonase endonuclease (Sigma) and 0.5% sodium deoxycholate. The virus containing supernatant was filtered using a 0.45m syringe and rAAVs were purified using an 15–54% Iodixanol density step gradient according Christensen et al. (2010).[60] rAAVs were titrated using rt-qPCR and used at 10,000 multiplicity of infection (MOI).

### Cell culture

Unless otherwise stated cell culture media solutions were purchased from Invitrogen. Cell lines; N2A neuroblastoma and HEK293T cells were maintained in DMEM supplemented with 10% fetal bovine serum (FBS), 1mM glutamine, 100U/mL penicillin and 100 μg/mL streptomycin in a humidified incubator with 5% $CO_2$ at 37°C.

*Primary neuronal cell culture*

Primary cortical and hippocampal neurons were derived from NMRI mice at embryonic day 16 (E16) according to Animal Welfare regulations. Pregnant mice were obtained from Charles River Laboratories (Sulzfeld, Germany). Brain tissue was dissected in HBSS medium supplemented with 1mM sodium pyruvate, 0.1% glucose and 10mM HEPES (pH7.3) and neurons were dissociated using 0.025% Trypsin. Neurons were seeded onto cell culture dishes (Falcon) or nitric-acid washed glass coverslips (Carl Roth GmbH) coated with 0.5 mg/mL poly-D-lysine (Sigma) in plating medium (Basal medium Eagle's containing Eagle's salts, 0.45% glucose, 10% horse serum (Capricorn; HOS-1A), 1mM sodium pyruvate, 100U/mL Penicillin and 0.1 mg/mL Streptomycin. Plating medium was replaced with serum-free maintenance medium MEM supplemented with 0.6% glucose, 0.2% sodium bicarbonate, 1mM sodium pyruvate, 2% B27 supplement (Gibco), 2mM Glutamax, 100U/mL Penicillin and 0.1 mg/mL Streptomycin. Neurons were kept in a humidified incubator supplied with 5% $CO_2$ at 37°C.

For microfluidic separation of neurites, hippocampal neurons were plated in one chamber of a two-part (XC150, Xona) or three-part (TCND1000, Xona) microfluidic device as per manufacturer instructions. Fluidic separation was achieved by directing flow toward the EV-treated chamber prior to and for the duration of the experiment.

*Cell culture treatments and transfection*

Recombinant BDNF (Peprotech, #450-02) was dissolved in sterile water containing 0.1% BSA. Neurons were treated with 50 ng/mL BDNF or control vehicle for 20–30min unless otherwise stated, and washed out 3 times with maintenance medium. Recombinant myc and myc-BDNF were from Chromotek and Cusabio, respectively. For blocking MAPK activity, neurons were treated with 10 μM

U0126 for 30min before addition of BDNF or control vehicle. Dynasore was dissolved in DMSO and used at 40 $\mu$M, 30min prior to addition of EVs. GW4869 was used at 5 $\mu$M. TTX and bicuculline were used at a concentration of 1 $\mu$M and 40 $\mu$M, respectively. AraC was applied on 1DIV at a concentration of 2 $\mu$M and washed out 24 h later. Lipofectamine 2000 reagent was used to transfect primary hippocampal neurons and N2A neuroblastoma cells according to manufacturer's instructions.

### Organotypic slice culture

Organotypic hippocampal slices were taken from P4-P5 NMRI mice according to the protocol of De Simoni et al. (2006).[61] Briefly, sagittal slices were obtained in slicing medium (Earle's Balanced Salt Solution, 25mM HEPES pH7.3) at 4°C using a vibratome (Leica VT1200S) and the hippocampus was dissected out. Hippocampal slices were transferred plated on 0.4$\mu$m-pore hydrophilic PTFE membrane Millicell culture plate inserts (Millipore) and maintained in MEM culture medium containing Earle's Balanced Salt Solution, 1mM Glutamax, 25% (w/w) Horse Serum, 100U/mL Penicillin and 0.1 mg/mL Streptomycin, pH7.4, in a humidified incubator at 37°C and 5% $CO_2$. Slices were used in experiments after 5–6 DIV.

## Protein analysis

Donor cells were washed thrice in cold PBS and lysed in CHAPS buffer (1% CHAPS, 5mM EDTA and 50mM Tris-HCl (pH8)). Post-nuclear supernatants were isolated by centrifugation at 4,500x$g$ for 10 min at 4°C. For quantification of protein concentration, EV pellets were lysed in CHAPS buffer (EVs from 100,000 donor cells/$\mu$l CHAPS) by vortexing at full speed for 2min and cell and EV lysates were subjected to Bicinchonic acid (BCA) assay.

### Immunoblotting

Cell lysates or EV pellets were re-suspended in Laemmli sample buffer by vortexing, and heated at 70°C for 10min before being subjected to SDS-PAGE electrophoresis. Proteins were transferred onto polyvinylidine difluoride (PVDF) membranes, which were blocked in Tris-buffered saline containing 0.1% Tween 20 and either 4% semi-skimmed milk powder or 5% BSA for phospho-specific antibodies. Antibodies were diluted in blocking buffer. HRP-conjugated secondary antibodies were purchased from JacksonImmuno Research. Blots were detected using the ChemiDoc MP imaging system (Bio-rad).

## EV isolation

EVs were isolated and characterized according to quality guidelines by the International Society of Extracellular vesicles.[62] For all experiments, fresh, serum-free collection medium was added to donor cells 16 h before EV isolation. Unless otherwise stated, 5-7DIV primary cortical neurons were used as sEV donors and 6-7DIV hippocampal neurons were EV recipients. For functional experiments, sEV stock concentration was 150 ng EV protein/$\mu$l (EVs from 100,000 donor cells/$\mu$l) and a final concentration of 3 $\mu$g EV protein/mL was used, unless otherwise specified.

### Differential ultracentrifugation (UC)

Unless otherwise stated, all steps were carried out on ice or at 4°C. Collected cell culture supernatants were centrifuged as depicted in Figure S1A. For mEV isolation, 10,000x$g$ pellets were washed once in cold PBS and centrifuged again for 30 min at 10,000x$g$. For sEV isolation, 10,000x$g$ supernatants were transferred to thickwall polyallomer tubes (Beckman Coultier) and subjected to UC for 1h at 100,000x$g$ in a fixed-angle rotor (rotor; TLA 100.3, $k$-factor; 48, Optima MAX-XP tabletop ultracentrifuge, Beckman Coulter). sEV pellets were washed in cold PBS by vortexing before the second UC step. UC supernatants were discarded by decanting. EV pellets were re-suspended in 20mM HEPES-buffered saline (pH7.4) containing 0.025% Tween 20 (Hepes-t) and protease inhibitors by gentle shaking for 20 min at room temperature.

For fluorescent labeling of sEVs, 100,000x$g$ pellets from the first UC step were re-suspended in HEPES-t and incubated with 100nM lipilight (Idylle, previously known as membright[38]) for 3min, after which sEVs were diluted 15-fold in PBS and pelleted again by UC. No-cell controls were processed in parallel, using non-conditioned cell culture medium.

For proteinase and RNAse treatment, sEVs pellets were re-suspended after the first UC step and sequentially treated with 10 $\mu$g/mL RNAse A for 10 min at 37°C, and 0.008% Trypsin for 5min, 37°C. EVs were then diluted in PBS by 100-fold and sujected to a second UC step.

### Size exclusion chromatography (SEC)

Isolation of sEVs by SEC was performed using 10,000x$g$ supernatants (Figure S1A) and qEVoriginal (70nm) columns (IZON Bioscience), according to manufacturer's instructions. Fractions of interest were pooled together and concentrated using 3 kDa ultra-filtration devices (Amicon).

## Nanoparticle tracking analysis (NTA)

NTA was performed on NanoSight NS500 LM10 instrument and an LM14 viewing unit equipped with a 532nm laser (NanoSight Ltd). Five 60-s measurements per sample were used for analysis using NTA 2.3 software. Values were normalized to relative protein concentration of donor neurons.

## RNA isolation

Total RNA was isolated using peqGOLD Trifast (VWR) and miRNeasy or RNeasy kits (Qiagen) for RNA sequencing experiments. Genomic DNA contamination was eliminated using either TURBO DNA-free kit (AM1907) or on-column digestion with RNAse-free DNAse set (Qiagen), respectively. RNA concentration was quantified using Nanodrop spectrophotometer.

## Whole cell transcriptomics

### RNA sequencing

Hippocampal neurons (6-7DIV) were treated with either Ctrl, BDNF, Ctrl-EV or BDNF-EV as described, and RNA was isolated 24 h later. The RNA sequencing library was prepared using the TrueSeq RNA library prep kit v2 (Illumina, USA) according to the manufacturer's protocol using 500ng total RNA. The quality of the libraries was assessed using the Bioanalyzer (Agilent Technologies) and library concentration was determined using the QubitTM dsDNA HS Assay Kit (Thermo Fisher Scientific, USA). Multiplexed libraries were directly loaded onto an Ilumina Hiseq2000 using a 50 bp single read setup. Demultiplexing was performed using Illumina CASAVA version 1.8. Sequencing adapters were removed using Cutadapt-1.8.1 software.

### Differential expression analysis

Raw counts were normalized to library size and converted using log2 transformation. Samples of low quality ($Z$ score >2.5 or $Z$ −2.5) were identified as outliers and excluded from further analysis. Only transcripts with read counts of more than 10 in at least 50% of the samples were used. The data was corrected for undesired variance due to batch effect using the RUVSeq package1.[58] DESeq22 was used to conduct differential expression analysis. The threshold for differentially expressed RNAs was set to log2(fold change) > 0.2 and p value <0.01 for sEV-treated samples and log2(fold change) > 0.378 and adjusted p value <0.05 for BDNF and Ctrl-treated samples.

## Small RNA sequencing

Twelve small RNA libraries representing 2 biological and 3 technical replicates from control- or BDNF-treated cortical neurons and corresponding sEVs were prepared using NEBNext Multiplex Small RNA Library Prep Set for Illumina (New England Biolabs) as per manufacturer's instructions and sequenced in Illumina HiSeq2000. An in-house developed pipeline was used to analyze the small RNAome. Quality check and demultiplexing were performed using the CASAVA 1.8.2 software (Illumina). To quantify small RNAome, reads were first mapped to mature miRNA sequences obtained by miRBase (http://www.mirbase.org/) followed by further mapping to other small non coding RNA sequences (http://www.ensembl.org/info/data/ftp/index.html). Reads were then mapped to the mm10 reference genome. Target prediction and gene set enrichment analysis was preformed using miRWalk (https://www.mirwalk.umm.uni-heidelberg.de/)[63,64]

## Gene ontology and pathway analysis

The DAVID[3] package[65,66] was used to generate the Gene Regulatory Network (GRN) for deregulated genes. The significance of each term was determined using a two-sided hypergeometric test, and the p value was corrected using Benjamini-Hochberg.

## Real-time quantitative PCR (rt-qPCR)

Reverse transcription was carried out using iScript cDNA synthesis kit (170–8891, Bio-Rad) for mRNA targets and TaqMan Advanced miRNA cDNA synthesis kit (ThermoFischer; A28007) for miRNAs. PCRs were performed on StepOnePlus Real-Time PCR system (Applied Biosystems) using either iTaq SYBR Green Supermix with ROX (Biorad, #172–5121) or TaqMan Fast Advanced Master Mix (ThermoFischer, #4444557) for TaqMan assays. For NGS validation, miScript II RT kit synthesis was used for cDNA synthesis and candidate miRNA-specific primers were used in SYBR Green-based PCR.

## Immunofluorescence

Neurons were fixed in 4% paraformaldehyde/4% sucrose/1x phosphate buffered saline (PBS) solution for 15–20 min at room temperature. For immunocytochemistry experiments, cells were permeabilized in 0.1% Triton X-100 for 5min, washed in PBS and immunostained with primary and secondary antibodies diluted in 2% BSA/0.1% Tween 20/1xPBS. To image sEVs in recipient cells, permeabilization was performed using 0.25% Saponin/5% BSA/PBS for 30 min at room temperature, and the same solution was used for primary and secondary antibody incubation. Primary antibodies were added onto glass coverslips for either 1 h at room temperature or overnight at 4°C, and Alexa-Fluor secondary antibodies (Thermo Scientific, 1:2,000) were incubated for 45–60 min at room temperature in a light-protected, humidified chamber. Slices were fixed in 4% PFA and cold 20% Methanol and permeabilized in 0.5% Triton X-100 for 18 h at 4°C. Non-specific binding was blocked using 20% BSA and antibodies were diluted in 5% BSA. Coverslips and slices were mounted on imaging slides using Mowiol 4–88 solution containing DABCO (24 mg/mL) and DAPI (1:10,000). Images were acquired on Zeiss LSM880 confocal microscope.

## Scanning transmission electron microscopy (STEM)

Glow-discharged formvar/carbon-coated TEM grids (400 mesh, copper) were floated on 20 μL drops of sEV samples for 10min. After removing excess solution, the grids were floated on 2% uranyl acetate for 30min. Afterward the staining solution was removed by dabbing the grids onto filter paper. TEM grids were further dried for at least 1 h before imaging on a Gemini II SEM column (Zeiss Crossbeam 550) at 30kV and 150pA (high resolution imaging mode) with an STEM detector. Quantification of particle size and number was performed in ImageJ[56] particle analyzer using thresholded images (ROI; 1,14 μm$^2$). Parameters were set to exclude particles less than 75nm or present at the edges of the field of view.

### Image analysis

#### Dual-fluorescence sensor assay

N2a cells were co-transfected with sensor plasmids and 10nM miRNA inhibitors and sEVs were added 24 h later. Cells were fixed after approximately 22–24 h. XY images were acquired using a 20× objective with picture tiling on two regions of interest (ROI). Sensor repression was quantified by randomly selecting 50–60 GFP-expressing cells and calculating the proportion of cells co-expressing dsRed. GFP cells were selected blindly, prior to red channel visualization.

#### Quantification of dendrite complexity

XY scans of dsRed-expressing neurons were acquired using a 20× objective and dendrite complexity was quantified using Sholl analysis. Concentric circles were placed around the neuronal soma at 15 $\mu$m intervals (end radius of 190 $\mu$m), and the number of intersections between the circles and neuronal dendrites was counted in thresholded images using the Sholl analysis plugin in ImageJ. The number of intersections was quantified for approximately 10 neurons per condition and averaged for each independent experiment.

#### Synapse density and pre-synaptic clustering analysis

XY scans were acquired using a 63× objective at optimal resolution parameters. The density of pre- and post-synaptic markers and the number of synapses was quantified in primary or secondary dendrites of similar thickness using a rectangular ROI of 20 × 8$\mu$m in ImageJ. Approximately 2–3 ROIs were averaged for each neuron in three independent experimental trials. Co-localization analysis was performed using Imaris 9.7 Coloc extension (ROI, 135 $\mu$m$^2$). Optimized channel thresholding was performed for each channel and kept constant across conditions and experimental trials. For quantification of pre-synaptic clustering, MAP2-labeled dendrites and SV markers were segmented using *Surfaces* in Imaris 9.7 and classified according distance from the dendritic surface (<2 $\mu$m) (ROI, 80 $\mu$m$^2$). For synapse quantification in slice cultures, XYZ images were acquired using a 40× objective and the number of overlapping PSD95 and SYP structures within 2 $\mu$m from MAP2-labelled dendrites was quantified in Imaris 9.7.

For synaptic dye uptake experiments, neurons were treated in high KCl Tyrode's solution (60mM KCl, 67mM NaCl, 2mM CaCl2, 2mM MgCl2, 30mM Glucose, 25mM HEPES, pH7.4) containing 10 $\mu$M FM1-43Fx, 50 $\mu$M APV, and 20 $\mu$M CNQX for 1 min and allowed to recover for 5 min in normal Tyrode's solution containing FM1-43Fx, prior to washing with 0 Calcium Tyrode's solution containing 1 $\mu$M TTX, 50 $\mu$M APV and 20 $\mu$M CNQX for 15 min. Synaptic dye uptake was quantified as FM1-43Fx mean intensity values overlapping with SYP-positive puncta in Imaris.

#### Calcium imaging

For calcium imaging experiments, hippocampal neurons were plated onto $\mu$Slide 8 well chambers (Ibidi) and transduced with AAV1-NES-R-Geco1a[54] or AAV1-GCAMP6S[53] and AAV-mCherry at 5DIV. EVs were added on 7DIV and cells were imaged on 10–11DIV on the Zeiss Cell Discover 7 at 37°C and 5% CO$_2$, using a 20x (0.95NA/0.5x) or 50x (1.2NA/1×) objectives. Images were acquired on a CCD camera at 0.3s intervals for 5 min for synaptic calcium transients and 0.5s intervals for 10 min for analysis of somatic transients. For synaptic transients, cells were placed in Tyrode's solution without Magnesium and in the presence of TTX (1 $\mu$M) and mean gray values were extracted from regions of interest (ROI) at spines as indicated by mCherry fluorescence and the presence of opposing SYP puncta in each of 3 independent experiments using Fiji. GCAMP6 values were normalized to mCherry fluorescence. For somatic transients, mean gray values were extracted from somatic and corresponding background ROI (ROI; 5 × 5$\mu$m) from 60 to 100 cells per chamber in Fiji. For each ROI, background fluorescence was subtracted from somatic fluorescence and divided by their sum. Changes in fluorescence ($\Delta F/F_0$) were calculated by defining $F_0$ as the mean of the smallest 20% of all values in a time series. Resulting traces were detrended using linear regression and Peaks were detected based on the threshold of 3x the standard deviation above baseline using the *Scipy* peak finder. Pearson's correlation coefficients were calculated for each neuron using the *Pandas* correlation function.

### Quantification of neuronal activity using multi-electrode arrays (MEA)

Hippocampal neurons were drop-plated onto the micro-electrode surface (1mm$^2$) of a CytoView 24-well MEA plate containing 16 electrodes, at a density of 20,000 neurons per well. Recordings were performed at a sampling frequency of 12.5 kHz for the duration of 20min (Maestro Edge, Axion Biosystems, Atlanta, GA). Spikes were detected by an adaptive threshold of 6.5 x standard deviation and bursts were defined by a maximum inter-spike interval of 100ms and at least 5 spikes per burst from a single electrode. Network activity was averaged in four wells per condition in each independent experiment. Recording and data analysis was performed using AxIS software (Axion Integrated Studio Navigator 1.5., Axion Biosystems). Neurons were treated with sEVs obtained from Ctrl or BDNF-treated 5-6DIV cortical neurons. For GW4869 treatments, 5 $\mu$M GW4869 was added to conditioning medium following a 20min incubation with Ctrl or BDNF (50 ng/mL).

### QUANTIFICATION AND STATISTICAL ANALYSIS

Data are represented as mean ± standard deviation, unless otherwise stated. Statistical significance tests were performed as indicated in the figure legends using GraphPad Prism software. All imaging experiments were performed in a blinded manner using at least 10 cells per experimental condition and independent trial. Volcano plots depict median (solid lines) and upper and lower quartiles (dashed lines). Python 3 was used for Calcium imaging analysis.[57] R statistical language (version 3.5.2) and R packages; DESeq2, RUVSeq2 and pheatmap were used for analysis of RNA sequencing data.